minerals

MDPI

Article

Metallogeny of Low-K Tholeiitic Magmas in Volcanic Arcs: Inferences from Petrology, Geochemistry and Micromineralogy of the Modern Mutnovsky Volcano Lavas (Kamchatka, Russia)

Nadezhda Potapova, Pavel Kepezhinskas * and Nikolai Berdnikov

Institute of Tectonics and Geophysics, Russian Academy of Sciences, Khabarovsk 680000, Russia; nadya.kozhemyako.22@mail.ru (N.P.); nick@itig.as.khb.ru (N.B.)
* Correspondence: pavel_k7@yahoo.com

Abstract

Metallogeny of low-K tholeiitic magmas in volcanic arcs is poorly documented and understood. The Mutnovsky volcano in Kamchatka erupted low-K tholeiitic basalt, basaltic andesite, andesite and dacite formed through partial melting of a depleted mantle wedge beneath the active front of the Kamchatka arc, followed by fractional crystallization in subarc magmatic conduits. Mineral microinclusions in Mutnovsky lavas are dominated by Cu-Ag chlorides and sulfides (±cerussite, baryte, cassiterite and Sb oxide), which show, along with the bulk rock Ag, Sn and Sb concentrations, a general increase during magmatic differentiation. Mutnovsky rocks are characterized by higher cumulative proportions of Cu-Ag sulfides and chlorides in comparison with the neighboring rear-arc Gorely and Bakening volcanoes, emphasizing the importance of S- and Cl-bearing fluids for their metallogenic evolution. Microinclusions in Mutnovsky tholeiites display certain similarities with ore mineral associations from epithermal and porphyry deposits in Kamchatka. Together with the enrichment of Mutnovsky lavas in Ag, Cu and Sb in reference to the bulk continental crust, this indicates a potential link between low-K tholeiitic magmas and Cu-Ag (±Sb, Sn) mineralization in volcanic arcs.

Keywords: volcanic arcs; Kamchatka; Mutnovsky volcano; low-K tholeiites; mineral microinclusions; metallogeny

1. Introduction

Modern volcanic arcs often contain epithermal and porphyry-style Cu-Ag-Au deposits, typically associated with pre-Quaternary volcanic and volcanic–sedimentary complexes [1–5]. Precious metal mineralization is commonly linked to the complex magma plumbing systems beneath arc volcanoes [6,7] and is accompanied by intense hydrothermal alteration [8,9]. Numerous field, geochemical and experimental studies suggest that copper, gold and silver are delivered into the ore-forming upper crustal environments in volcanic arcs by magmatic–hydrothermal fluids exsolved from the metal-rich arc magmas originating from a variety of lithospheric sources [10–12]. The metals are partitioned into parental magmas during partial melting of subarc mantle and crustal sources or scavenged by upwelling magmas from the metal-bearing rock complexes (mineralized paleo-systems) in the underlying island arc crust [13,14]. Magmatic differentiation in long-lived subarc magma chambers and conduits results in accumulation of precious metals in sulfur- and chlorine-rich melts and high-temperature fluids, which, upon separation from the residual

Academic Editor: Massimo D'Antonio

Received: 26 February 2026
Revised: 19 March 2026
Accepted: 19 March 2026
Published: 21 March 2026

silicate liquids, transport ore components into shallow, subvolcanic porphyry and epithermal environments [15,16]. The final metal precipitation and formation of economic deposits are dictated by a variety of structural and physico-chemical factors that belong to low-temperature and low-pressure geologic environments and ore-forming processes [17,18].

Although general metallogenic features of volcanic arc magmas are well-documented [6,7,13,16,19,20], the relative roles of magmatic versus hydrothermal processes in ore genesis in volcanic arcs remain the subject of ongoing debate. Multiple studies suggest that elevated water content and the oxidized state of arc magmas play an important, if not crucial, role in their ability to dissolve and carry ore metals such as gold, silver, copper, etc. [19,21,22]. Several other studies indicate that ore metal behavior in arc magmas is influenced by contents and activities of minor components, such as sulfur, chlorine and carbon dioxide [13,23,24]; rates and duration of crustal magma fluxes [11,25]; and additional tectonic factors, such as crustal thickness, geometry of arc-related fault systems, and depth and duration of metal-rich magma fractionation [7,8,26]. This is consistent with elevated concentrations of sulfur and chlorine in melt inclusions from some subduction-related magmas associated with epithermal and porphyry mineralization [13,27]. High concentrations of H_2O, S and Cl have been detected in melt inclusions in basalts, andesites and dacites from several Kamchatka volcanoes, suggesting their overall mineralizing potential [28,29]. Kamchatka contains numerous Cu-Ag-Au porphyry and epithermal deposits and showings associated with Late Cenozoic arc volcanism [5,30]. However, specific details about metallogenic connections between arc volcanoes and mineralization in Kamchatka, the exact nature of metal enrichment and sources of metals in arc magmas, as well as ore metal behavior and mobility during their crustal differentiation, require further clarification and delineation.

In this paper, we present new mineralogical and geochemical data for a suite of differentiated volcanic rocks from the Mutnovsky volcano in the southern Kamchatka arc in an attempt to address the following issues: (1) document metal and mineral microinclusions in rock-forming minerals and groundmass glass and evaluate the role of magmatic and post-magmatic processes in their formation; (2) determine concentrations and distribution of chalcophile metals in a suite of basaltic and andesitic rocks from a typical arc volcano; and (3) outline principal metallogenic features of volcanic arc magmas in relation to the magmatic and post-magmatic phases of their differentiation and emplacement in the upper crust.

2. Geologic Background

The Kamchatka volcanic arc records multiple episodes of Cenozoic subduction, arc-related volcanism and terrane accretion in the northwestern corner of the Pacific Ocean [31–35]. The Kamchatka arc is segmented (Figure 1) into: (1) the northern inactive segment associated with Miocene subduction of the Komandorsky Basin oceanic crust [33]; (2) the central segment with two sublatitudinal volcanic chains (the Eastern Volcanic Front and the remnant Sredinny Range) separated by the active intra-arc rift of the Central Kamchatka Depression; and (3) the southern segment, which is a structural and stratigraphic continuation of the intraoceanic Kurile arc separated from the central and northern segments by the Petropavlovsk–Malkinsky Fracture Zone. The modern calc-alkaline and tholeiitic volcanism within the central and southern segments of the Kamchatka arc is associated with the subduction of the Mesozoic Pacific plate beneath the eastern edge of the Okhotsk microplate along the Kurile–Kamchatka deep-sea trench [31,34,35].

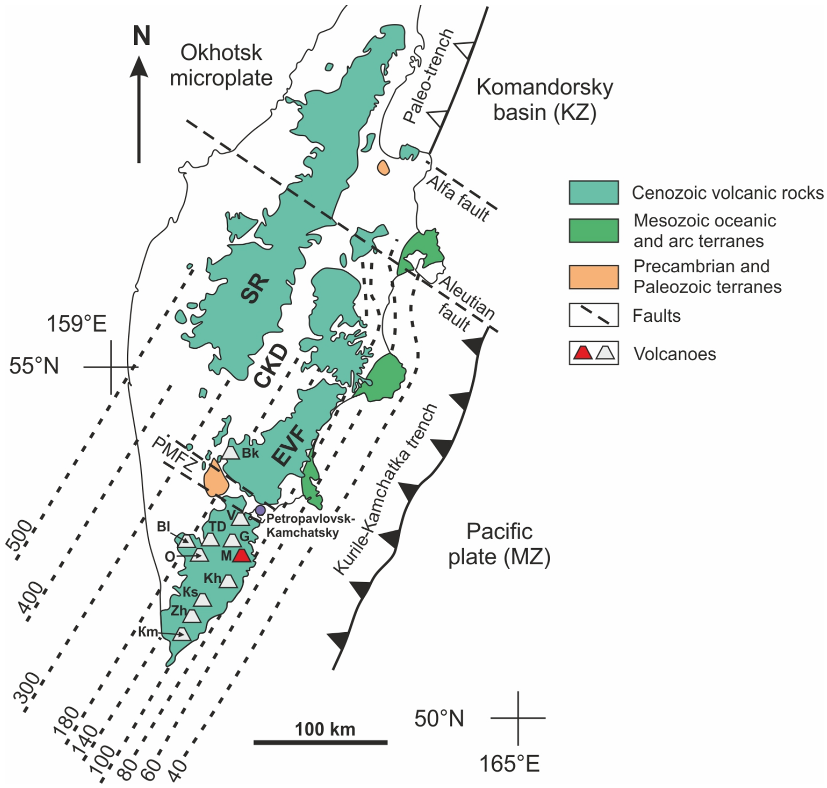

Figure 1. Tectonic setting of the Kamchatka volcanic arc showing the location of the Mutnovsky volcano (filled red triangle) and the surrounding eruptive centers, modified from [30,35]. Principal arc segments: SR—Sredinny Range, CKD—Central Kamchatka Depression, EVF—Eastern Volcanic Front. Volcano abbreviations: M—Mutnovsky, G—Gorely, V—Vilyuchinsky, TD—Tolmachevsky Dol, O—Opala, BI—Bolshaya Ipelka, Kh—Khodutka, Ks—Ksudach, Zh—Zheltovsky, Km—Kambalny. PMFZ—Petropavlovsk–Malkinsky Fracture Zone. Depth to the subducted slab in km (short, dashed contours) is from [36].

The Mutnovsky volcano is located within the Eastern Volcanic Front (EVF) of the southern Kamchatka segment at the easternmost tip of the cross-arc volcanic chain composed of the rear-arc-front Gorely volcano, the areal volcanism of the Tolmachev Dol, the Opala caldera and the back-arc shield volcano of Bolshaya Ipelka (Figure 1). The P-wave velocity structure of the mantle wedge below the Mutnovsky volcano suggests that it is positioned, like most arc front volcanoes in Kamchatka, approximately 90–100 km above the subducting slab [36]. Mutnovsky consists of four coalesced composite cones (Mutnovsky I, II, III and IV), which have been active since the Late Pleistocene [37]. Mutnovsky I and II cones, together called "Old Mutnovsky", formed between 80 and 30 ka and produced over 80 km^3 of basalt, basaltic andesite, andesite and minor dacite lava and pyroclastic rock. The "Younger Mutnovsky" cones III and IV erupted mostly basalts and basaltic andesites with some minor andesite and dacite extrusions in the course of the last 15 ka of the Mutnovsky volcano evolution [37]. The youngest historic eruption in March 2000 produced basaltic andesite scoria and pyroclastic material. The Mutnovsky volcano is associated with a very active magmatic–hydrothermal system, and its active Mutnovsky IV crater emits volcanic gases at temperatures of ~620 °C, contributing approximately 80 percent to the total volcanic output [38]. Sublimates from the high-temperature (470–507 °C) fumarolic gases at Mutnovsky contain sulfides, sulfosalts, halides and sulfohalides of cadmium, lead and bismuth [39]. Detailed geochemical investigations indicate the lack of any significant variations in lava compositions from all four Mutnovsky cones [36]. We sampled several representative basalt, basaltic andesite and andesite lava flows across the Mutnovsky

I–III volcanic edifices for the purpose of the detailed metallogenic study of this typical arc-related volcano.

3. Materials and Methods

All analytical work was carried out at the Khabarovsk Innovation–Analytical Center (KhIAC) of the Institute of Tectonics and Geophysics (Far East Branch of the Russian Academy of Science, Khabarovsk, Russia).

A petrographic study of volcanic rocks was carried out using the Imager A2m microscope (Carl Zeiss, Jena, Germany). Investigation of morphology and chemical composition of minerals, mineral microinclusions, native metals and their alloys was conducted using a Vega 3 LMH (TESCAN, Brno, Czech Republic) scanning electron microscope (SEM) equipped with an X-Max 80 (Oxford Instruments, Abingdon, UK) energy-dispersive spectrometer (EDS) with the following operating conditions: accelerating voltage of 20 kV, beam current of ~500 nA and beam diameter of 0.2 μm. An extensive database of reference samples for all chemical elements incorporated into the Advanced AztecEnergy 2.0 software was used as standards during our SEM study. Accuracy of the EDS analyses was estimated to be ±0.1 wt.%. X-ray spectra of microinclusions of less than 5 μm in size, besides the spectral response from the inclusion itself, typically include some excitation spectra from a host mineral. A correction method proposed in [40,41] was used to interpret mixed spectra for ultra-small metal and mineral microinclusions. Mineral identification and its indexation on BSE images were conducted on the basis of peculiarities of their individual SEM-EDS spectra. In the case of the stoichiometric mineral compositions, individual minerals were identified in BSE images with abbreviated symbols according to the nomenclatures outlined in [42,43]. In more complex cases, the multi-component mineral phases were identified in the microphotographs with tabulated component contents in wt.%, followed by some interpretations in figure captions and relevant parts of the text.

Major elements were measured on pressed pellets using an S4 Pioneer XRF spectrometer (Bruker, Leipzig, Germany). International LDI-3 (gabbro) and WMG-1a (mineralized gabbro) reference materials were used for calibration. The analytical accuracy for major elements was ±10% [44]. Abundances of trace elements were determined with an ELAN 9000 ICP-MS spectrometer (Perkin Elmer, Woodbridge, ON, Canada) after the acid digestion of a powdered sample. In addition to the above-listed standards, geochemical reference samples BHVO-2 (USGS, Reston, VA, USA; Hawaiian basalt) and JB-3 (Geological Survey of Japan; Fuji basalt), along with Perkin Elmer standard solutions for internal calibration, were used to control the accuracy of analytical measurements. The accuracy was ±5% for trace element abundances of >20 ppm and ±10% for chemical elements with abundances of <20 ppm [44].

4. Results

4.1. Petrography of Volcanic Rocks

Basalts, basaltic andesites and andesites at the Mutnovsky volcano form characteristic massive lava flows, sometimes with a blocky appearance and jagged or clinkery surface. Dacites are present either as short, thick vesicular lava flows or extrusive domes and plugs within the partially eroded older Mutnovsky caldera. All studied samples are very fresh, and any secondary alteration is limited to a very spotty saussuritization of some plagioclase phenocrysts and localized occurrence of clay minerals in the glassy groundmass of a few lava flows.

Basalts are typically porphyritic with phenocrysts (~10–15% of the total rock volume) composed of olivine, plagioclase and minor clinopyroxene (Figure 2A). Groundmass displays a typical microlitic texture. Olivine forms small euhedral phenocrysts and microphenocrysts with rare spinel inclusions and embayments of groundmass volcanic glass. Euhedral plagioclase phenocrysts are typically characterized by sharp optical zoning and irregular distribution of melt and fluid inclusions (Figure 2A). In most cases, melt inclusions dominate the cores of large plagioclase crystals, but they are also occasionally observed within the thin outer rims. Augitic clinopyroxene forms euhedral to anhedral microphenocrysts occasionally intergrown with plagioclase. Accessory minerals include magnetite, spinel, ilmenite and rare apatite.

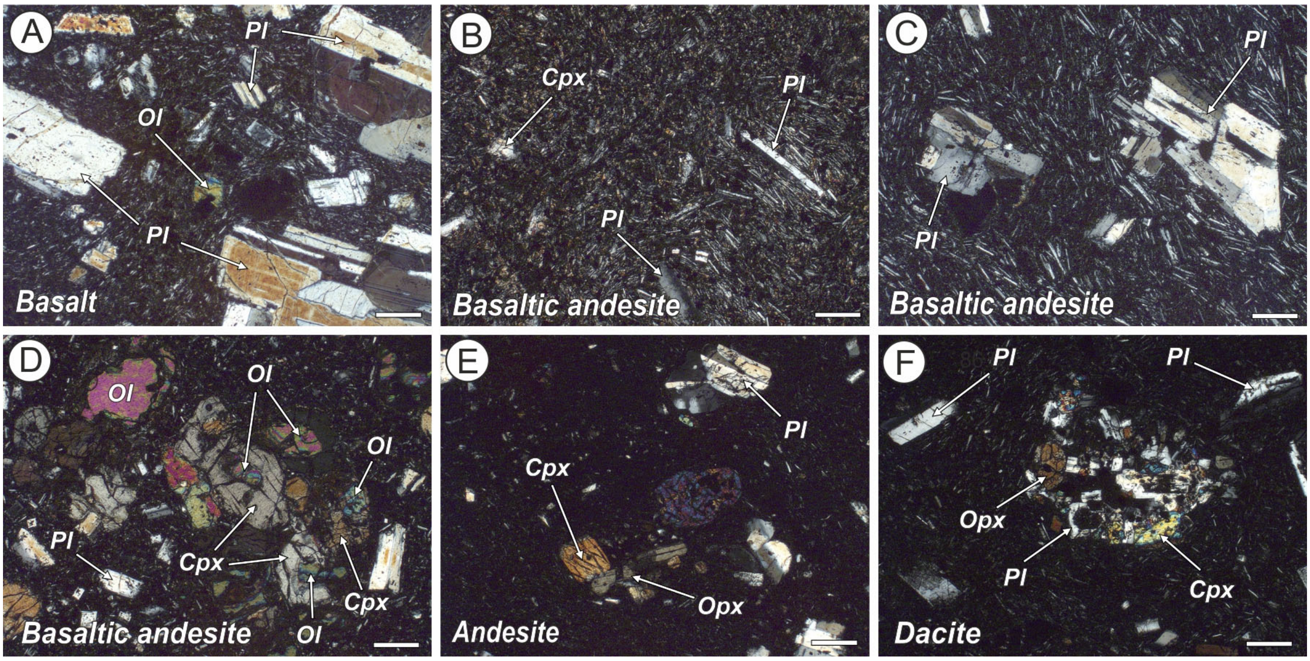

Figure 2. Petrographic features of the Quaternary lavas from the Mutnovsky volcano. (**A**) Porphyritic basalt with microlitic groundmass texture. (**B**) Aphyric to weakly porphyritic basaltic andesite with hyalopilitic groundmass. (**C**,**D**) Porphyritic basaltic andesite with microlitic groundmass texture. (**E**) Weakly porphyritic andesite with hypocrystalline groundmass. (**F**) Hypocrystalline dacite with a crystal clot composed of plagioclase, orthopyroxene and clinopyroxene. All microphotographs were taken in cross-polarized light. Ol—olivine, Opx—orthopyroxene, Cpx—clinopyroxene, and Pl—plagioclase. The scale bar in all photos is 20 μm.

Basaltic andesites display aphyric (Figure 2B), plagioclase–phyric (Figure 2C) and olivine–clinopyroxene–plagioclase–phyric (Figure 2D) textures. Groundmass textures in basaltic andesites from the Mutnovsky volcano range from microlitic to hyalopilitic and typically are macroscopically similar to more mafic lavas. Aphyric basaltic andesites are highly vesicular (up to 20–30%) and contain rare microlites and microphenocrysts of equant clinopyroxene as well as needle-like plagioclase laths (Figure 2B). Accessory minerals are mostly titanomagnetite and apatite. Phenocrysts in porphyritic basaltic andesite 7-93 are dominated by calcic plagioclase, which occasionally shows crude optical zoning with both cores and rims carrying elongated melt inclusions (Figure 2C). Titanomagnetite inclusions are also present in some plagioclase cores. Other accessory minerals include apatite and rare Ti-poor magnetite. Olivine- and clinopyroxene-bearing basaltic andesites from the Mutnovsky volcano typically carry unzoned euhedral to anhedral phenocrysts and microphenocrysts of olivine and clinopyroxene in addition to unzoned to weakly zoned plagioclase with very thin outer rims (Figure 2D). Olivine also occurs as inclusions in clinopyroxene, and both minerals frequently form bimineralic crystal clots up to 100–300 microns in size (Figure 2D). Some clinopyroxene phenocrysts also contain inclusions of unzoned euhedral plagioclase. Magnetite (both Ti-rich and Ti-poor compositional varieties) is the main accessory mineral in olivine-bearing basaltic andesites from the Mutnovsky volcano.

Andesite lava from the Mutnovsky III stratocone is characterized by porphyritic texture composed of clinopyroxene, orthopyroxene and plagioclase phenocrysts in a hypocrystalline groundmass (Figure 2E). Plagioclase is typically unzoned, and pyroxenes frequently form small clusters and intergrowths of euhedral prismatic microphenocrysts (Figure 2E). Accessory minerals are represented by Ti-enriched magnetite and minor needle-shaped apatite.

Dacite from the Mutnovsky III cone has a generally vesicular and sparsely phyric appearance with a few unzoned euhedral plagioclase laths scattered around the volume of this volcanic rock (Figure 2F). Crystal clots (100–200 microns in size) composed of plagioclase, orthopyroxene and clinopyroxene, as well as amphibole microphenocrysts, are observed in the hypocrystalline groundmass of Mutnovsky dacite. Both Ti-rich and Ti-poor magnetite, minor apatite and rare zircon are principal accessory minerals in this felsic lava.

4.2. Geochemistry of Volcanic Rocks

Major (wt.%) and trace element (including ore metals; ppm) concentrations in Quaternary lavas from the Mutnovsky volcano are listed in Table 1.

Table 1. Major (wt.%) and trace (ppm) element concentrations in Quaternary lavas from the Mutnovsky volcano.

Sample	**MTN-4**	**MTN-6**	**MTN-5**	**MTN-7**	**MTN-3**	**MTN-2**	**MTN-1**
Rock type	Basalt	Basaltic andesite	Basaltic andesite	Basaltic andesite	Basaltic andesite	Andesite	Dacite
SiO_2	52.14	53.20	54.51	54.67	55.88	62.33	63.56
TiO_2	0.99	1.31	1.16	1.43	0.97	0.91	0.60
Al_2O_3	18.41	16.11	15.03	16.94	15.96	15.77	16.38
Fe_2O_3	10.43	12.39	11.26	11.74	10.07	7.49	5.93
MnO	0.18	0.20	0.18	0.21	0.16	0.13	0.12
MgO	3.61	3.91	3.36	2.70	3.30	1.39	1.06
CaO	9.90	8.62	8.66	8.25	8.82	6.61	4.77
Na_2O	2.49	2.70	2.61	2.99	2.62	3.07	4.24
K_2O	0.38	0.42	0.37	0.41	0.61	1.66	1.87
P_2O_5	0.15	0.19	0.18	0.20	0.17	0.16	0.20
LOI	1.02	0.34	2.54	0.18	0.94	0.36	1.30
Total	99.69	99.40	99.85	99.72	99.50	99.86	100.02
Cr	52.25	51.54	45.38	34.74	75.81	109.45	54.50
Ni	7.57	8.04	6.20	4.41	24.27	10.72	4.84
Co	26.57	29.76	23.88	24.21	28.12	17.26	18.74
V	262.51	294.71	236.31	256.54	198.30	141.04	88.71
Sc	26.82	30.01	25.88	30.32	22.41	18.07	10.80
Li	2.92	5.20	6.08	6.14	4.09	13.18	6.27
Cs	0.16	0.43	0.41	0.38	0.42	2.12	1.29
Rb	3.08	5.30	5.00	3.78	6.47	30.06	23.30
Ba	133.49	920.92	166.13	160.00	211.72	405.05	369.52
Sr	352.59	336.67	315.59	342.09	333.36	309.43	246.04
Zr	38.72	52.76	44.09	50.02	51.23	118.64	55.05
Y	15.47	20.63	17.04	25.23	15.94	24.28	13.07
Nb	0.89	0.98	1.13	0.77	1.29	2.57	1.76
Ta	0.24	0.32	0.20	0.16	0.26	0.34	0.46
Hf	1.28	1.76	1.42	1.75	1.55	3.78	1.74
Th	0.37	0.31	0.52	0.29	0.51	2.16	1.94
U	0.17	0.15	0.19	0.14	0.22	0.95	0.84
La	3.98	4.79	5.16	5.87	6.02	11.35	7.64
Ce	10.25	12.91	12.70	13.84	14.40	26.35	16.21

https://doi.org/10.3390/min16030332

Table 1. *Cont.*

Sample	MTN-4	MTN-6	MTN-5	MTN-7	MTN-3	MTN-2	MTN-1
Pr	1.77	2.32	2.17	2.81	2.30	4.00	2.32
Nd	8.48	11.45	10.02	13.81	10.32	17.04	9.58
Sm	2.55	3.49	2.89	4.24	2.82	4.42	2.45
Eu	0.89	1.18	1.00	1.35	0.95	1.13	0.83
Gd	3.07	4.11	3.48	4.99	3.36	5.03	2.76
Tb	0.53	0.72	0.59	0.87	0.56	0.83	0.45
Dy	2.97	4.05	3.29	4.84	3.05	4.55	2.49
Ho	0.67	0.92	0.75	1.10	0.69	1.03	0.55
Er	1.85	2.53	2.08	3.02	1.95	2.85	1.57
Tm	0.29	0.39	0.32	0.46	0.30	0.45	0.26
Yb	1.79	2.37	1.91	2.81	1.80	2.74	1.67
Lu	0.29	0.39	0.32	0.46	0.29	0.45	0.28
Cu	16.45	106.54	99.34	91.58	71.89	59.82	20.09
Zn	49.50	81.49	60.88	68.04	54.63	56.49	63.40
Mo	0.62	0.68	0.58	0.68	1.13	2.16	1.00
Ag	0.39	0.30	0.25	0.63	0.39	0.48	0.38
Sn	0.76	1.12	0.62	0.81	0.84	1.24	2.65
Sb	0.42	0.23	0.12	0.34	0.17	0.66	0.40
As	1.29	1.41	1.34	1.67	1.38	1.26	1.33
Pb	2.33	3.67	3.13	3.21	3.75	7.85	6.59
Cd	0.06	0.09	0.08	0.09	0.11	0.06	0.06
Bi	<0.001	<0.001	<0.001	<0.001	<0.001	0.03	0.02

4.2.1. Major and Trace Elements

Quaternary lavas from the Mutnovsky volcano are characterized by variable TiO_2 contents, which decrease from basalt to dacite, coupled with generally low MgO and elevated Al_2O_3 concentrations (Table 1). Mutnovsky lavas plot into the subalkaline basalt, basaltic andesite, andesite and dacite fields in the TAS classification diagram (Figure 3A). Basalt and basaltic andesites are characterized by low K_2O contents and plot into the low-K tholeiitic field in the K_2O-SiO_2 discrimination graph, while andesite and dacite samples exhibit slightly elevated potassium concentrations and plot in the calc-alkaline field in the same diagram (Figure 3B). Mutnovsky lavas largely display tholeiitic differentiation character in the AFM space, with the two most evolved compositions (andesite MTN-2 and dacite MTN-1; Table 1) plotting on the discrimination line between the tholeiitic and calc-alkaline magmatic series (Figure 3C). Primitive mantle-normalized incompatible trace element patterns for the Mutnovsky lavas display profound depletions in high-field strength elements (HFSE; Nb and, in most cases, Zr) and general enrichment in large ion lithophile elements (LILE) such as Cs, Rb and Ba (Figure 3D). The latter is also characterized by a pronounced positive anomaly of different amplitudes. Sr also exhibits detectable enrichments in all samples in reference to both the HFSE and light rare-earth elements (LREE; Figure 3D). These geochemical features are characteristic of the volcanic front lavas with tholeiitic differentiation tendencies in modern volcanic arcs worldwide.

4.2.2. Ore Elements

Quaternary lavas from the Mutnovsky volcano are characterized by elevated concentrations of some ore elements, such as molybdenum, silver, tin and antimony (Table 1). Copper and zinc are generally present at the levels typical of subduction-related volcanic rocks, and bismuth is below the detection limits of the ICP-MS method in all samples except the two most evolved ones (andesite MTN-2 and dacite MTN-1; Table 1). The behavior of the ore elements in the Mutnovsky lavas is illustrated in Figure 4, where their concentrations are plotted against the silica content of the studied samples. Several chalcophile elements, especially molybdenum (Figure 4A), tin (Figure 4D), antimony (Figure 4E) and lead (Figure 4F), show the tendency to increase with the increasing silica content of host volcanic rocks. Arsenic and silver show considerable scatter with a generally detectable tendency for a slight increase in silver (Figure 4B) and a decrease in arsenic (Figure 4C) concentrations. Cadmium contents are identical in basalt, andesite and dacite (Cd = 0.06 ppm; Table 1) and somewhat elevated (Cd = 0.08–0.11 ppm; Table 1) in all basaltic andesite lavas from the Mutnovsky volcano.

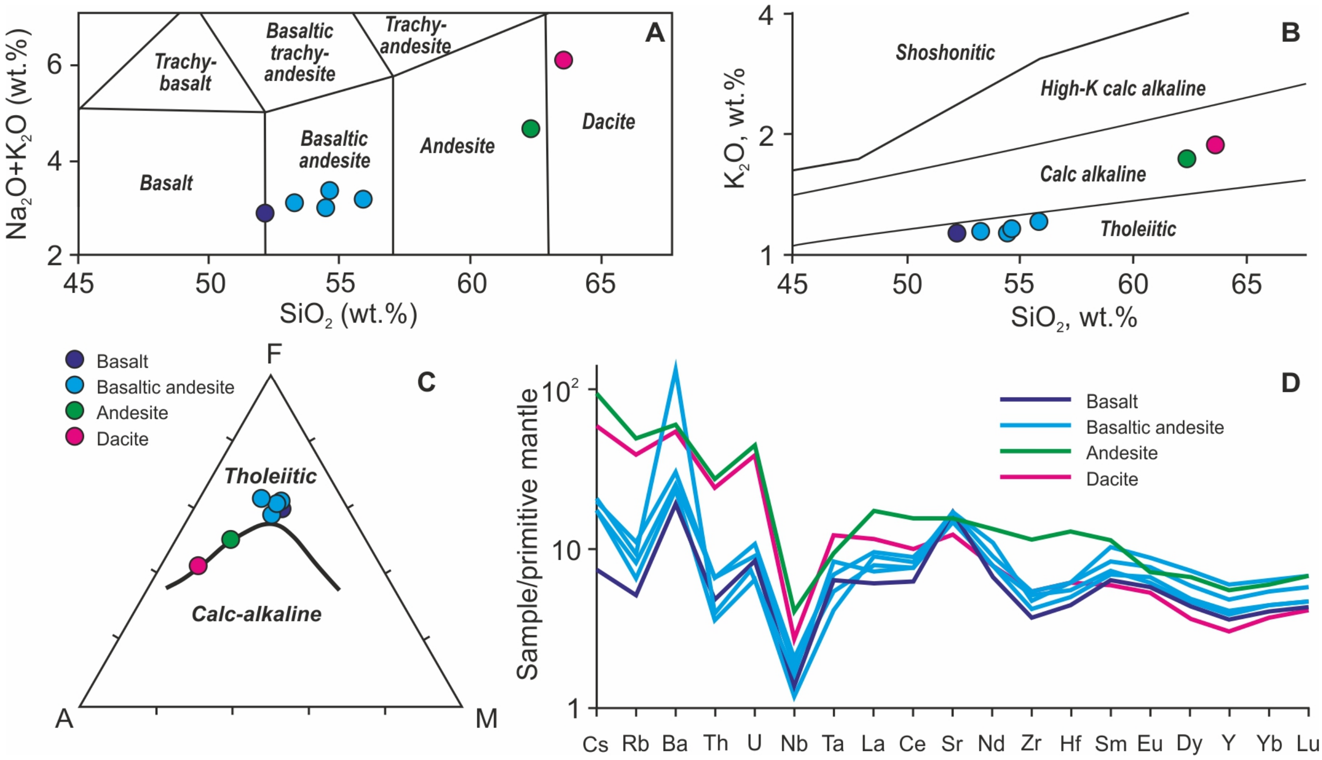

Figure 3. Major and trace element composition of the Quaternary Mutnovsky lavas. (**A**) The total alkalies–silica (TAS) diagram is from [45]. (**B**) The K_2O-SiO_2 discrimination graph is from [46]. (**C**) Na_2O+K_2O (A)–total FeO (F)–MgO (M) diagram. The discrimination line between the tholeiitic and calc-alkaline series is from [47]. (**D**) Primitive mantle-normalized trace element patterns for Mutnovsky lavas. Normalizing values are from [48].

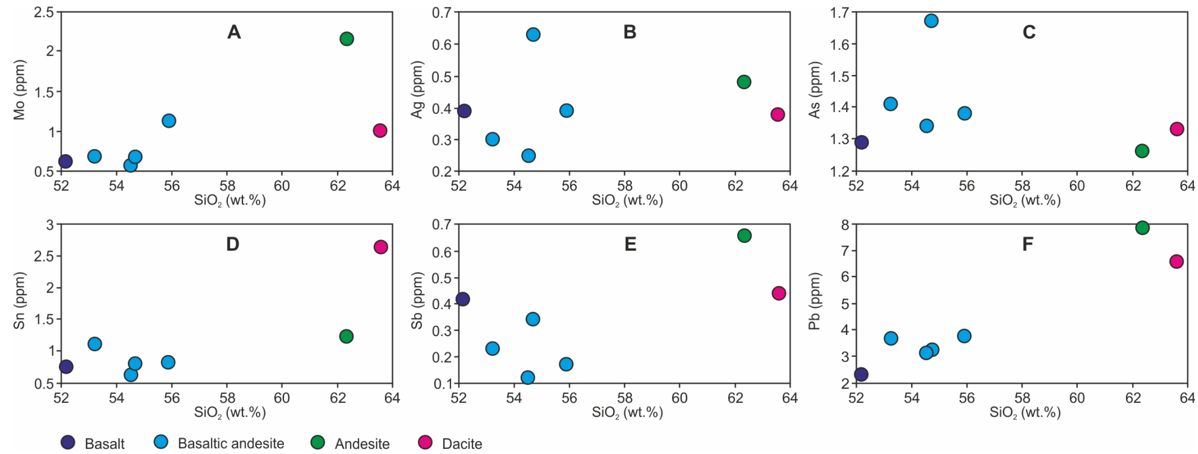

Figure 4. Co-variation of SiO_2 (wt.%) with molybdenum (**A**), silver (**B**), arsenic (**C**), tin (**D**), antimony (**E**) and lead (**F**) in Quaternary lavas from the Mutnovsky volcano.

4.3. Metal and Mineral Microinclusions

Young volcanic rocks from the Mutnovsky volcano contain microinclusions of metals and minerals represented by (1) alloys of chalcophile metals; (2) micrograins of Ag-Cl composition; (3) metal–chlorine–sulfur-bearing composites; (4) acanthite; (5) composite copper and silver sulfides; (6) oxides; (7) sulfates; and (8) carbonates and zeolites.

Chalcophile metal alloys in differentiated tholeiitic lavas from the Mutnovsky volcano are represented by anhedral microinclusions of natural bronze in amphibole (Figure 5A) and natural brass in plagioclase (Figure 5B) from basalt, as well as an equant micrograin of cupriferous silver in plagioclase from basaltic andesite (Figure 5C).

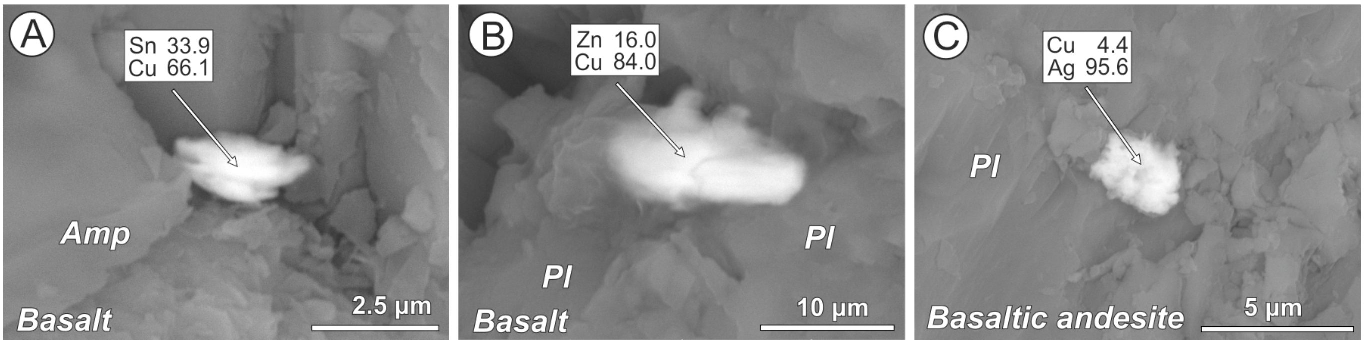

Figure 5. Backscatter electron (BSE) images of chalcophile metal alloys in Mutnovsky lavas. (**A**) Microinclusion of Sn-Cu alloy in amphibole. (**B**) Microinclusion of Zn-Cu alloy in plagioclase. (**C**) Microinclusion of Cu-Ag alloy in plagioclase. Amp—amphibole, Pl—plagioclase.

Ag-Cl microinclusions are characterized by an Ag/Cl ratio ranging from 8 to 16 and are most probably composed of a mixture of native silver and chlorargyrite. They typically occur as equant grains with a porous internal appearance in orthopyroxene (Figure 6A), plagioclase (Figure 6B) and amphibole (Figure 6C) from basalt; anhedral, slightly more homogeneous microparticles in orthopyroxene (Figure 6D), plagioclase (Figure 6E,F) and groundmass volcanic glass (Figure 6G) from basaltic andesites; and anhedral porous microinclusions in anorthoclase (Figure 6H) and amphibole (Figure 6I) from dacite. A compound microinclusion in orthopyrene (Figure 6D) is apparently an intergrowth of native silver with chlorargyrite and acanthite. Composite silver chlorides in basaltic andesites are occasionally associated with titanomagnetite (Figure 6F,G).

Mutnovsky lavas also contain composite microinclusions formed by intergrowths of native silver with chlorine-bearing and, occasionally, sulfur-bearing microminerals of copper and zinc (Figure 7). Physical mixtures of native silver with Cu-Ag (Figure 7A) and Zn-Ag (Figure 7B) chlorides are observed in plagioclase from basalt. Basaltic andesites from the Mutnovsky volcano carry composite microinclusions of native silver, silver chloride, acanthite, and, possibly, copper sulfide in plagioclase and orthopyroxene (Figure 7C–F).

Euhedral to anhedral microinclusions of acanthite are also observed in plagioclase from basalt (Figure 8A), basaltic andesite (Figure 8B) and dacite (Figure 8C) from the Mutnovsky volcano.

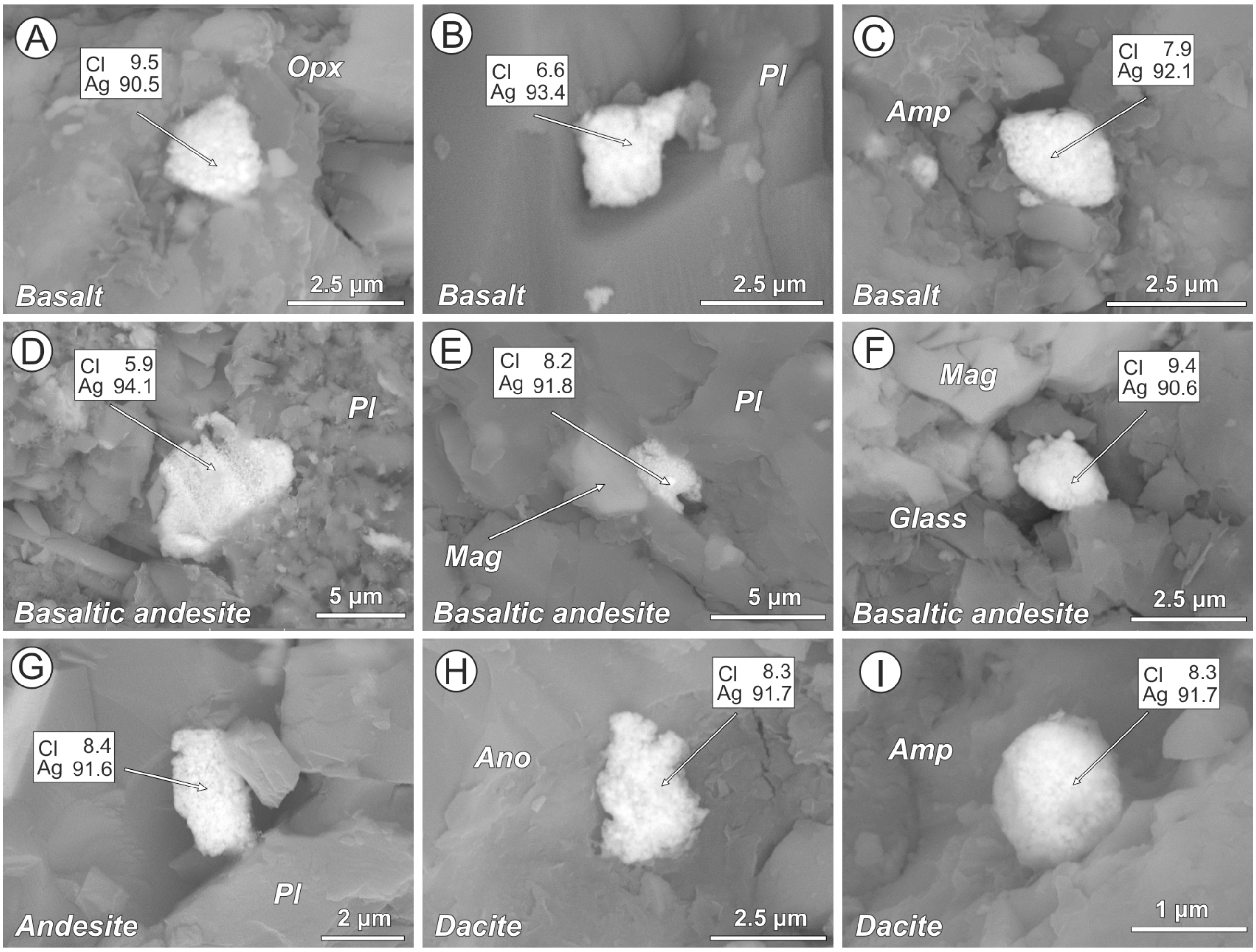

Figure 6. BSE images of Ag-Cl microinclusions in Mutnovsky lavas: (**A**–**C**) in orthopyroxene (**A**), in plagioclase (**B**), and in amphibole (**C**) from basalts; (**D**–**F**) in plagioclase (**D**), in plagioclase in association with Ti-magnetite (**E**), and in volcanic glass in association with Ti-magnetite (**F**) from basaltic andesites; (**G**) in plagioclase from andesite; and (**H**,**I**) in anorthoclase (**H**) and in amphibole (**I**) from dacite. Amp—amphibole, Ano—anorthoclase, Mag—magnetite, Opx—orthopyroxene, Pl—plagioclase.

Another common type of copper- and silver-bearing microminerals in Mutnovsky lavas is represented by intergrowths of acanthite with Cu sulfides (Figure 9). These composite inclusions are observed in plagioclase from basalt (Figure 9A); amphibole (Figure 9B), plagioclase (Figure 9C,D) and volcanic glass (Figure 9E) in the groundmass of the basaltic andesite; plagioclase (Figure 9F) and groundmass glass (Figure 9G) from andesite; and anorthoclase (Figure 9H) and volcanic glass (Figure 9I) in dacite. In several cases, the Cu-Ag sulfides form clusters of acicular microcrystals (Figure 9F,I). In two cases, Cu-Ag sulfides are associated with euhedral titanomagnetite microcrystals included in plagioclase (Figure 9D) and in volcanic glass (Figure 9E). Prismatic and rhombic microparticles of Cu-Ag sulfides are growing over a micrograin of Cu-Ag-S-Cl in amphibole (Figure 9B), which appear to be compositionally similar to Cu-Ag-S-Cl micrograins in Figure 7D,E. A composite sulfide of zinc, copper and silver in volcanic glass from dacite appears to be overgrown (covered) with acicular acanthite microparticles, which texturally resemble acicular acanthite microcrystals observed in basalt-hosted plagioclase grain (Figure 8A).

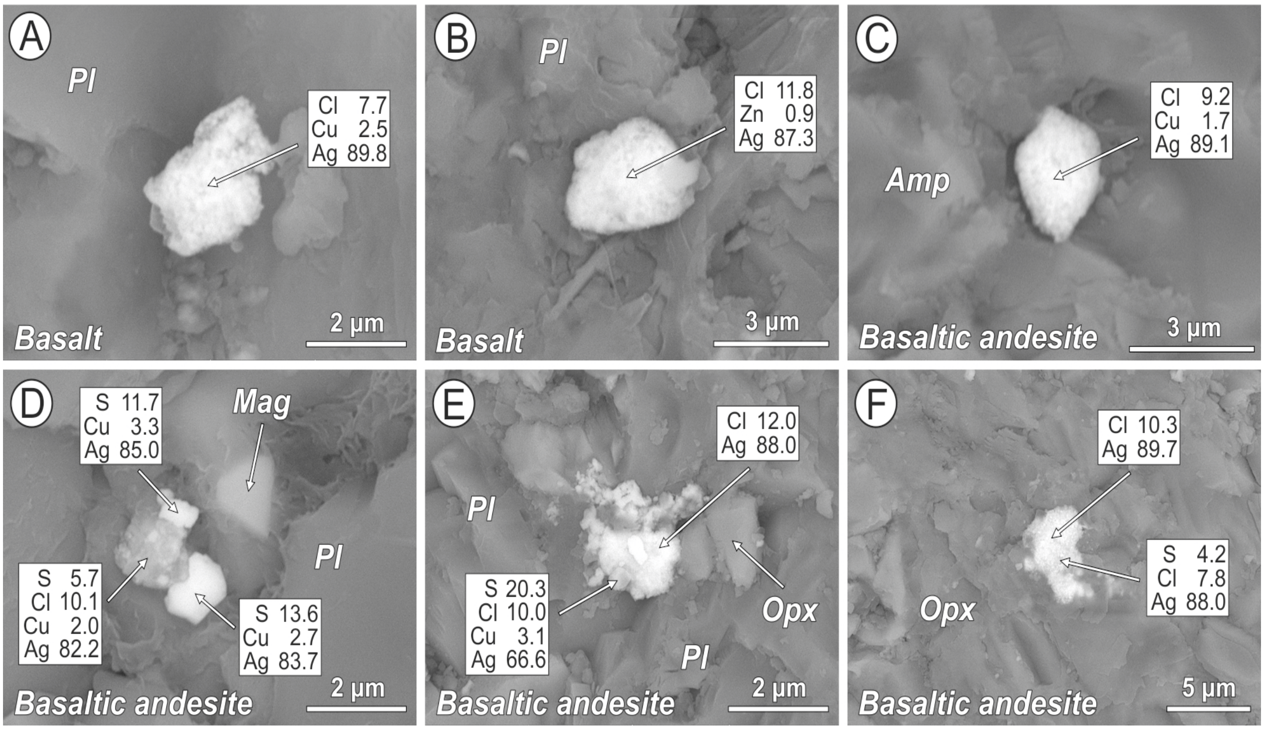

Figure 7. BSE images of composite metal–chlorine–sulfur-bearing microinclusions in Mutnovsky lavas. (**A**,**B**) composite microinclusions of native silver with Ag-Cu (**A**) and Ag-Zn (**B**) chlorides in plagioclase from basalt. (**C**–**F**) Composite microinclusion of native silver with Cu and Ag chlorides in amphibole (**C**); composite microinclusion of native silver, silver chloride and Cu-Ag sulfides in association with Cu-Ag sulfides and titanomagnetite in plagioclase (**D**); composite microinclusion of native silver, chlorargyrite, acanthite and Cu sulfide in orthopyroxene–plagioclase matrix (**E**); and composite microinclusion of native silver and chlorargyrite with minor acanthite (**F**) from basaltic andesite. Amp—amphibole, Mag—magnetite, Opx—orthopyroxene, Pl—plagioclase.

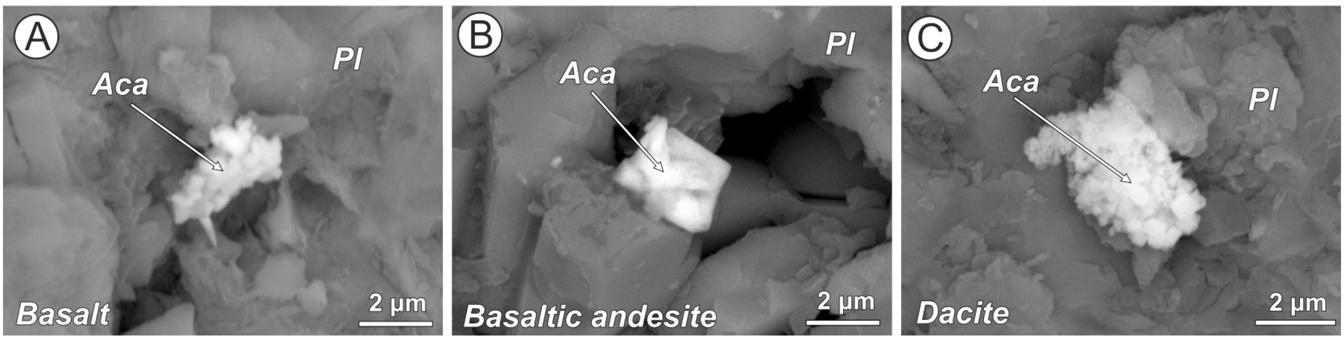

Figure 8. BSE images of acanthite microinclusions in Mutnovsky lavas. (**A**–**C**) Acanthite microinclusions in plagioclase from basalt (**A**), basaltic andesite (**B**) and dacite (**C**). Aca—acanthite, Pl—plagioclase.

Volcanic rocks from the Mutnovsky eruptive center also contain microinclusions of chalcophile metal-bearing oxides, carbonates and zeolites (Figure 10). Calcic plagioclase in basaltic andesites includes a cluster of prismatic and acicular micrograins of cassiterite (Figure 10A). An anhedral microparticle of Zn-bearing zeolite, compositionally comparable to gaultite ($Na_4Zn_2Si_7O_{18} \cdot 5H_2O$), is observed in plagioclase from basalt (Figure 10B). Sb oxide, compositionally similar to valentinite (Sb_2O_3), is also present in basalt-hosted plagioclase (Figure 10C). Euhedral equant (possibly twinned) and acicular microcrystals of cerussite ($PbCO_3$) are included in plagioclase (Figure 10D) and volcanic glass (Figure 10E) in dacite. Finally, an equant euhedral micrograin of bismite is present in quartz from the dacitic lava (Figure 10F).

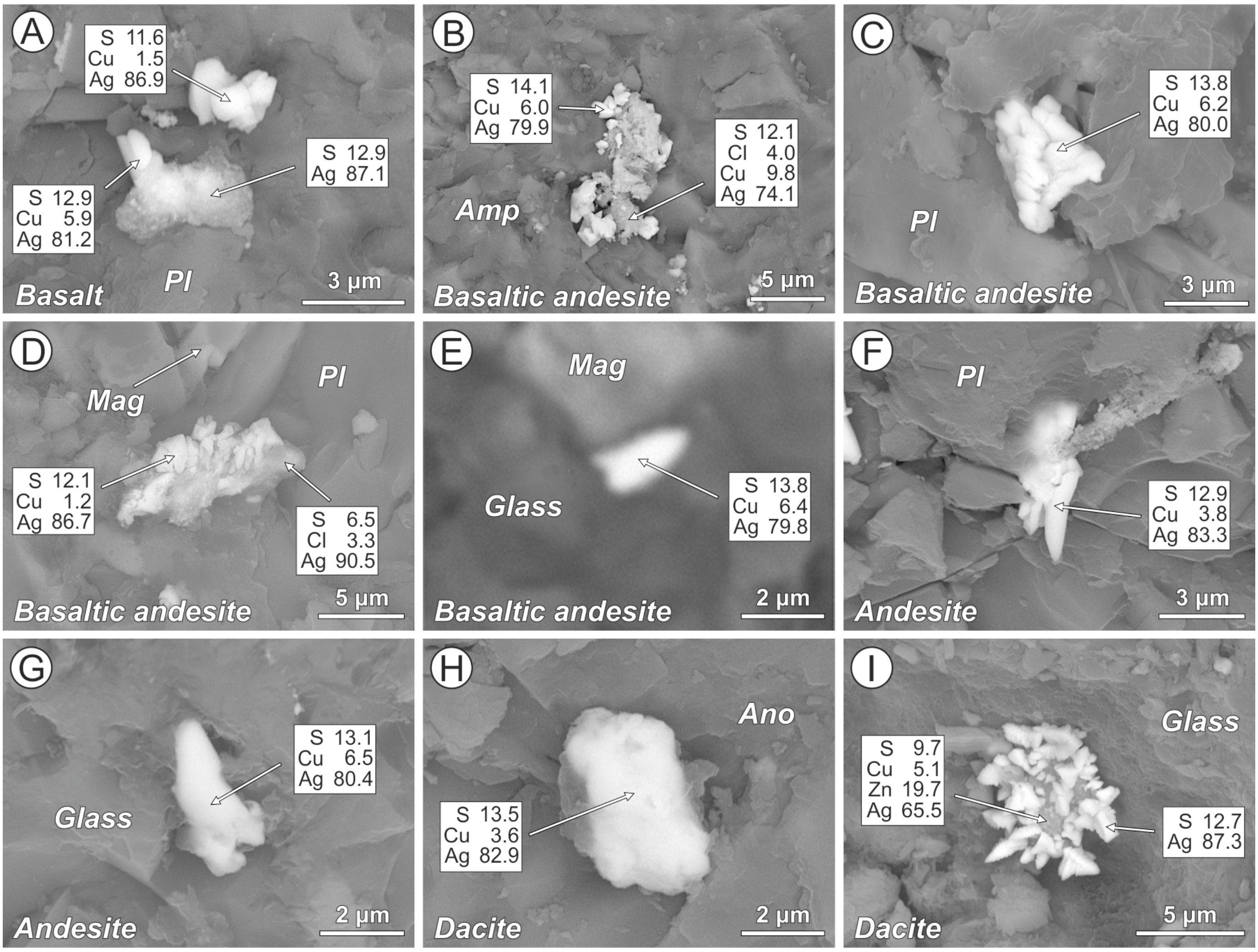

Figure 9. BSE images of copper and silver sulfides in Mutnovsky lavas. (**A**) Microinclusions of the composite Cu-Ag sulfides in plagioclase from basalt. (**B**–**E**) Microinclusions of Cu-Ag sulfides in association with Cu-Ag-Cl-S compound in amphibole (**B**), in plagioclase (**C**), in association with Ag-Cl-S compound and titanomagnetite in plagioclase (**D**), and in association with titanomagnetite in volcanic glass (**E**) from basaltic andesite. Microinclusion of Cu-Ag sulfide in plagioclase (**F**) and in volcanic glass (**G**) from andesite. Microinclusion of Cu-Ag sulfide in anorthoclase (**H**) and acanthite growing over the Ag-Cu-Zn-S composite in volcanic glass (**I**) from dacite. Amp—amphibole, Ano—anorthoclase, Glass—volcanic glass in the groundmass, Mag—magnetite, Pl—plagioclase.

Baryte microinclusions in lavas from the Mutnovsky volcano occur only in basalt and basaltic andesites, where they form either isolated anhedral grains in plagioclase (Figure 11A) or clusters of characteristic tabular microcrystals growing parallel to one another in host orthopyroxene grains (Figure 10B,C).

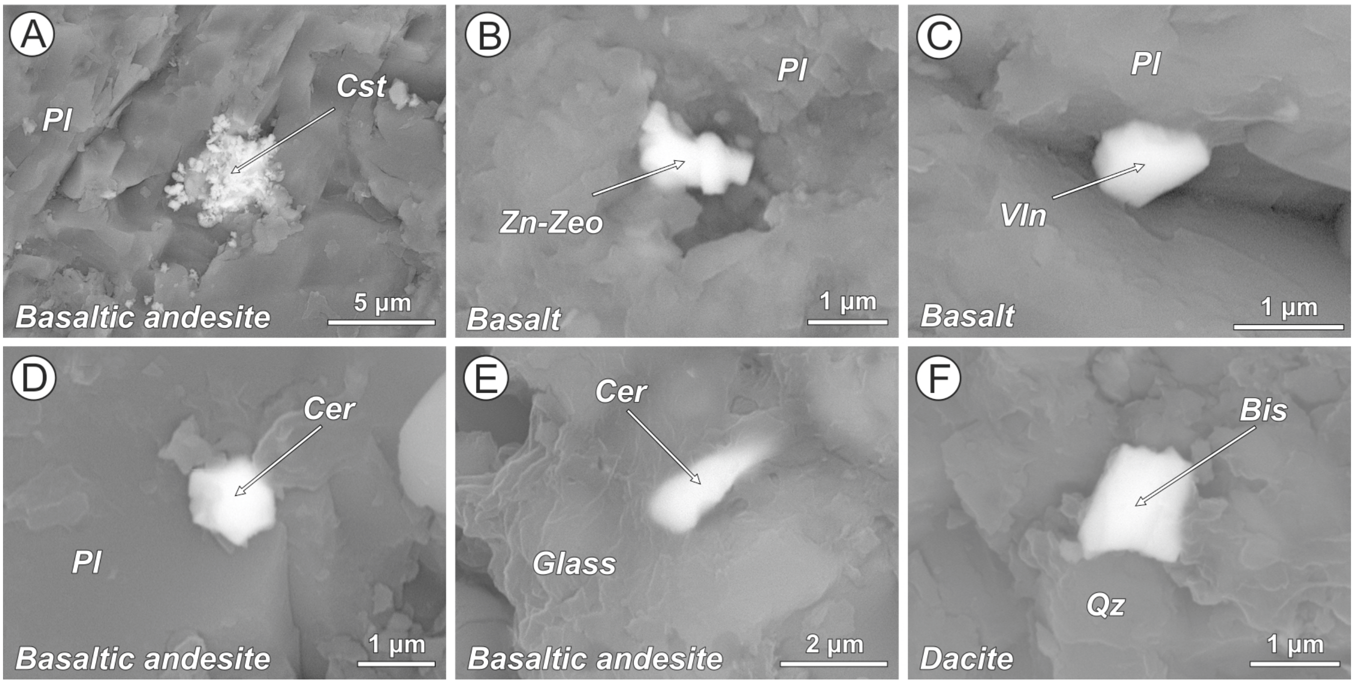

Figure 10. BSE images of oxide, carbonate and zeolite microinclusions in Mutnovsky lavas. (**A**) Cluster of cassiterite microcrystals in plagioclase. (**B**) Zn-bearing zeolite in plagioclase. (**C**) Valentinite (Sb_2O_3) in a fracture in plagioclase. (**D**,**E**) Cerussite microinclusions in plagioclase (**D**) and volcanic glass (**E**). (**F**) Bismite (Bi_2O_3) microinclusion in quartz. Bis—bismite, Cer—cerussite, Cst—cassiterite, Glass—volcanic glass, Pl—plagioclase, Qz—quartz, Vln—valentinite, Zn-Zeo—Zn-bearing zeolite.

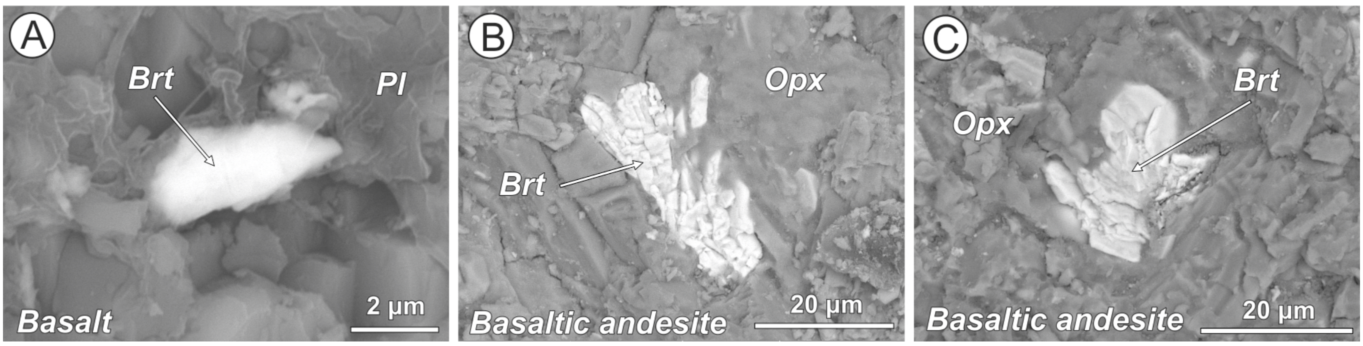

Figure 11. BSE images of baryte microinclusions in Mutnovsky lavas. (**A**–**C**) Baryte microinclusions in plagioclase from basalt (**A**) and orthopyroxene from basaltic andesite (**B**,**C**). Brt—baryte, Opx—orthopyroxene, Pl—plagioclase.

5. Discussion

Quaternary basalts, basaltic andesites, andesites and dacites from the Mutnovsky volcano display pronounced HFSE depletions coupled with LILE and LREE enrichments and follow tholeiitic differentiation trends typical of low-K volcanoes in some active volcanic arc fronts [49,50]. In many mineralogical and geochemical aspects, Mutnovsky lavas are similar to low-K, arc tholeiitic volcanic rocks, which erupted in several volcanoes within the Eastern Volcanic Front of Kamchatka [51,52]. Basalt and basaltic andesites from the Mutnovsky volcano are characterized by low K_2O contents (0.37–0.61 wt.%; Table 1; Figure 3B) and extremely low Rb/Y (0.15–0.41) and Nb/Y (0.03–0.08) typical of depleted N-MORB ([53,54]; Figure 12A). Samples of andesite and dacite share low MORB-like Nb/Y values (0.11 and 0.14) with less differentiated lavas but display higher Rb/Y ratios, indicating involvement of the subduction-related fluid component (Figure 12A). This is consistent with variable but generally high Ba/Yb ratios in Mutnovsky lavas (56.9–388.6), which, according to the geochemical model of [55], is in agreement with the substantial input (flux) of slab-derived volatiles into the depleted mantle source beneath the Mutnovsky volcano. The Sr, Nd, Pb and Hf isotope systematics further confirm this two-component (depleted mantle wedge source fluxed by LILE-enriched slab-derived fluid) model for the petrogenesis of the Mutnovsky lavas [35,36]. Variations of niobium and yttrium in Mutnovsky samples suggest their origin through a 10–25% partial melting of a strongly depleted mantle wedge source beneath the South Kamchatka volcanic front (Figure 12B). Basalts, basaltic andesites and andesites at the Mutnovsky volcano are linked via fractional crystallization of olivine, clinopyroxene and plagioclase from the parental basaltic magma [36]. Dacite lavas, which are volumetrically minor, display low overall concentrations of incompatible trace elements, especially rare earths (Table 1), and are best modeled "as the products of dehydration partial melting at mid-crustal levels of a garnet-free, amphibole-bearing basaltic rock, which itself formed in the mid-crust by emplacement of magma that originated from the same source as all Mutnovsky magmas" [36]. This is also consistent with the derivation of evolved Mutnovsky lavas from an N-MORB or a P-MORB-type basaltic source, as suggested by the Nb-Y relationships (Figure 12B). Fractional crystallization of parental basalt was apparently facilitated by the existence of well-developed, multi-level magma conduits beneath the Mutnovsky volcano, as indicated by the ambient noise tomography [56].

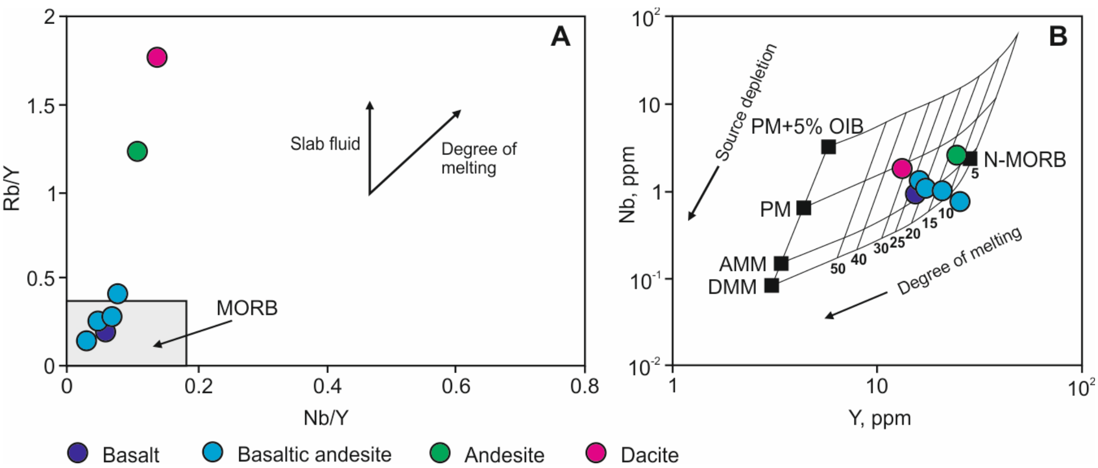

Figure 12. Trace element systematics of Mutnovsky lavas. (**A**) Rb/Y vs. Nb/Y. MORB field and chemical trends are from [35]. (**B**) Nb (ppm) vs. Y (ppm) modified from [52]. DMM—depleted MORB mantle and AMM—average MORB mantle from [53]; PM—primitive mantle, N-MORB—depleted mid-ocean ridge basalt, and OIB—ocean island basalt from [54].

Mutnovsky volcano hosts a very large and dynamic magmatic–hydrothermal system manifested in several active and fossil fumarole fields, which is also the site of the operating Mutnovsky geothermal plant [56,57]. Volcanic gases and associated fumarolic deposits at Mutnovsky volcano are enriched in SO_2, H_2S, HCl, Cu, Zn, Cd, Pb, Bi, As, Ag and Au, while high-temperature (470–507 °C) sublimates and encrustations contain abundant Cd-Pb-Tl halides, Pb-As-Bi sulfohalides and Cd-Pb-Bi-As sulfosalts [38,39,58] in association with baryte and various low-temperature sulfate minerals [59]. In addition, microinclusions (1 to 10 µm in size) of baryte, acanthite and chlorargyrite were observed in chemically homogeneous pyrite crystals in fumarolic exhalates [58].

5.1. Possible Role of Magmatic Differentiation

Since concentrations of some chalcophile metals in Mutnovsky lavas appear to vary with increased degree of differentiation (Figure 4), it is important to evaluate any potential changes in micromineral assemblages from the least fractionated basalts and basaltic andesites (MgO ~3 wt.%) to the more evolved andesite and dacite (MgO ~1–1.5 wt.%; Table 1). Assemblages of ore microminerals in Mutnovsky lavas exhibit some subtle variations during magmatic differentiation (Figure 13). For example, relative proportions of Ag and Cu-Ag sulfides (Figures 8 and 9) and, to a lesser extent, chalcophile (Cu, Sn, Zn, Ag) alloys (Figure 5) increase from basaltic to andesitic/dacitic compositions (Figure 13). This is consistent with the observed subtle increase in silver concentrations in some basaltic andesite and andesite lavas (Figure 4B). Silver behaves as an incompatible element during differentiation of intermediate and felsic magmas [60,61] and "efficient Ag partitioning into magmatic fluids will only take place when the composition of the silicate melt is felsic enough (rhyodacitic to rhyolitic)" [62]. Proportions of chlorine-bearing compounds (Figures 6 and 7) slightly decrease from basalt (Figure 13A) to basaltic andesite (Figure 13B) and more evolved lavas (Figure 13C), while composite Cl-S-bearing microinclusions (for example, Figures 7 and 9B,D,E) occur only in basaltic andesites (Figure 13B). Metasomatic mineral microinclusions (baryte, cerussite, and Zn-bearing zeolite; Figure 10), although not directly related to magmatic differentiation, are proportionally most common in basalt and basaltic andesites and do not occur in andesite and dacite lavas from the Mutnovsky volcano (Figure 13). This can be potentially explained by intense shallow degassing of mafic lavas immediately prior to and during their emplacement and cooling at the volcanic edifice of the Mutnovsky eruptive center [63].

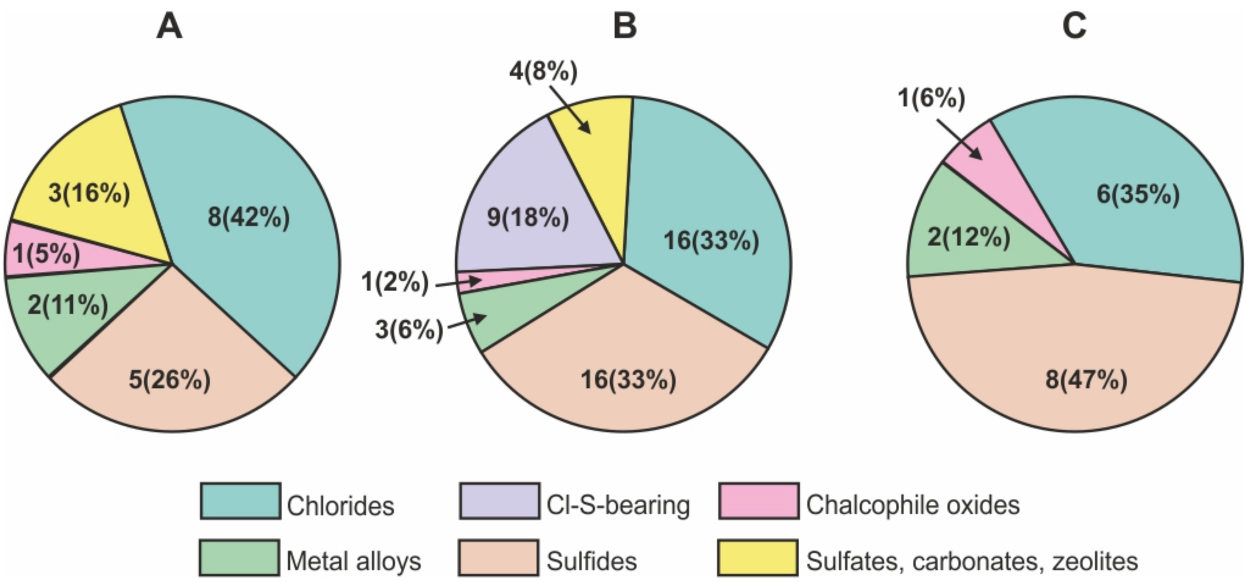

Figure 13. Distribution of metal and mineral microinclusions (number of the SEM-EDS analyses and their relative proportion in brackets) in basalts (**A**), basaltic andesites (**B**) and andesites/dacites (**C**) from the Mutnovsky volcano.

Changes in microinclusion assemblages from basalt to andesite and dacite are very subtle, but they may potentially reflect some differences in redox conditions and melt/fluid compositions during magmatic differentiation. For example, variations in relative proportions of chalcophile metal sulfides and chlorides from basalt to andesite/dacite in Mutnovsky lavas (Figure 13) may indirectly reflect variation in sulfur and chlorine contents in associated magmatic volatiles, which appears to be a common feature in volcanic arc magmas [64,65]. The general increase in Cl-bearing compounds (Ag-Cu-Zn chlorides + Ag-Cu-S-Cl compounds) from basalt to basaltic andesite is consistent with incompatible behavior of chlorine in fractionating volcanic arc magmas [64]. The total amount of chlorine-bearing microminerals in andesite and dacite (Figure 13C), which is comparable with that of basalt (Figure 13A), may either represent (record) buffering of chlorine concentrations through degassing processes that accompany differentiation in a shallow magma chamber beneath the Mutnovsky eruptive center [63] or reflect the initial chlorine content in a separate batch of felsic magma formed through partial melting of a mid-crust basaltic protolith [36]. Continuous expansion of chalcophile sulfides in comparison with the other types of ore microminerals in Mutnovsky lavas, accompanied by the increase in metal alloys and reduction in the amount of the oxidized sulfate (baryte) microinclusions (Figure 13), is consistent with elevated sulfur and reduced, or buffered, oxygen activities during magmatic differentiation. Based on their study of the climate-altering 1257 CE eruption of Mt. Samalas in Indonesia, Ding et al. suggested that "intermediate redox conditions, with sulfur as both sulfate and sulfide, and progressive magma recharge maximized pre-eruptive sulfur accumulation at Samalas" [66]. Overall, it is likely that physico-chemical conditions of the parental basaltic melt fractionation in a shallow, convecting magma chamber beneath the Mutnovsky volcano played an important formative role in the micromineral assemblages observed in the studied lavas.

5.2. Comparison with the Rear-Arc Volcanoes

The arc-front Mutnovsky volcano is part of a long (>100 km) cross-arc chain of stratovolcanoes (Gorely, Opala), areal cinder cones (Tolmachev Dol) and shield-type volcanoes (Bolshaya Ipelka) in the southern segment of the Kamchatka arc (Figure 1). Assemblages of microinclusions in the Mutnovsky and Gorely volcanoes, as well as another long-lived, rear-arc Bakening eruptive center, are summarized in Table 2.

Table 2. Comparison of ore microminerals in arc front (Mutnovsky) and rear-arc (Gorely and Bakening) volcanoes in Kamchatka.

Volcano	Tectonic Setting	Rock Types	Metal and Mineral Microinclusions	Host and Associated Minerals
Mutnovsky	Volcanic arc front	Basalt, basaltic andesite, andesite, dacite	Cu-Ag, Cu-Sn and Cu-Zn alloys; Cag + native Ag composites; Cu-Ag-Cl, Zn-Ag-Cl, Cu-Ag-Cl-S, Zn-Cu-Ag-Cl-S compounds; Cst; Bis; Cer; Vln	Ol; Cpx; Opx; Pl; Ano; Ab; Qz; Ap; Ti-Mag; Mag; Ttn; Brt; Zeo
Gorely	Rear arc	Basalt, basaltic andesite, andesite, dacite	Native Ag and Au; Cu-Ag, Cu-Sn, Cu-In-Sn and Fe-W alloys; Cag + native Ag composites; U-Ag-Cl, Cu-Ag-Cl; Cu-U-Ag-Cl-S, Cu-Ag-Sn-Cl-S, Cu-Ag-Sn-Cl and Cu-Ag-Cl-S compounds; Aca; Po; Gn; Cu-Ag sulfides; Ni-Cu-Fe sulfides; Cst	Ol; Opx; Cpx; Amp; Pl; Ano; Kfs; Bt; Ser; Ab; Qz; Ti-Mag; Mag; Ilm; Spl; Ap; Bdy; Zrn; Brt
Bakening	Rear arc	Dacite	Native Cu; Cu-Sn, Cu-Ag, Cu-Ag-Au and Ti-Co-W alloys; Ag-Cl, Cu-Cl, Cu-Ag-Cl-S compounds; Cu-Ag sulfides; Po; Py; Ccp; Bis; Cst; Znc; Cer; Str; Bmc	Opx; Amp; Bt; Pl; Ano; Qz; Ti-Mag; Mag; Ilm; Rt; Cr-Fe-Spl Cl-Ap; Bdy; Zrn; Brt; Mnz; REE-silicates

Note. Data sources: Mutnovsky, this study; Gorely [67]; Bakening [68]. Mineral abbreviations: Ab—albite, Aca—acanthite, Amp—Amphibole, Ano—anorthoclase, Ap—apatite, Bdy—baddeleyite, Bis—bismite, Bmc—bismoclite, Brt—baryte, Bt—biotite, Cag—chlorargyrite, Cal—calcite, Ccp—chalcopyrite, Cer—cerussite, Cpx—clinopyroxene, Cst—cassiterite, Gn—galenite, Ilm—ilmenite, Kfs—K-feldspar, Mag—magnetite, Mnz—monazite, Ol—olivine, Opx—orthopyroxene, Pl—plagioclase, Po—pyrrhotite, Py—pyrite, Qz—quartz, Ser—sericite, Spl—spinel, Str—strontianite, Ti-Mag—titanomagnetite, Ttn—titanite, Vln—valentinite, Zeo—zeolite, Znc—zincite, Zrn—zircon.

For comparative purposes, it is worth mentioning that both Mutnovsky and Gorely volcanoes erupted differentiated basalt–basaltic andesite–andesite–dacite series, while late-stage development of the Bakening center was marked by emplacement of hornblende dacites with adakitic geochemical characteristics [35]. Mafic and evolved lavas from all three volcanoes contain inclusions of metals and alloys, compounds of chlorine (±sulfur) with silver and other chalcophile elements (Cu, Zn, Sn), acanthite and Cu-Ag sulfides in association with baryte, cassiterite and other chalcophile sulfides, oxides and carbonates (Table 2). Cassiterite, which occurs as microinclusions in magmatic minerals such as Ca-plagioclase in all three volcanoes, is also reported from high-temperature (400–500 °C) fumarole sublimates at the Tolbachik volcano in central Kamchatka, where it was either directly deposited from the gas phase or formed via interaction of the host basaltic scoria with the high-temperature volcanic gases [69,70].

As opposed to the Gorely and Bakening centers, Mutnovsky lavas do not contain gold or gold-bearing alloys (Table 2). In addition, microinclusions, which compositionally resemble valentinite (Figure 10C), bismite (Figure 10F), cerussite (Figure 10D,E) and Zn-bearing zeolite (Figure 10B), are observed in some Mutnovsky samples. Most of these exotic mineral phases are found among exhalate assemblages in Kamchatka fumaroles. Cerussite occurs in the oxidizing Western (Mt. 1004 meters a.s.l.) paleo-fumarole field at the Tolbachik volcano in association with chalcophile metal chlorides, Cu oxides and Cu-Zn-Pb sulfates and arsenates [71]. Low-temperature cerussite also occurs in the Cl-rich fumarole field ("the Cotunnite Pit") associated with the 1944 eruption of the Vesuvius volcano in association with anglesite, atacamite, rare lead chlorides and oxychlorides (cotunnite, matlockite, napoliite, etc.) [72]. Although antimony oxides are so far not found in Kamchatka fumaroles, hematite from high-temperature (500–850 °C) sublimates in the Arsenatnaya fumarole at the Tolbachik volcano reportedly contains up to 2.6 wt.% of Sb_2O_5 [70]. Elevated antimony concentrations of up to 0.03 mg/kg were detected in high-temperature (410–507 °C) fumarolic condensates sampled from the active crater of the Mutnovsky volcano [39]. Zeolites, although not Zn-bearing ones, are common in hydrothermally altered rocks associated with hot springs and geysers at several volcanoes in southern (Kambalny, Koshelev) and central (Bolshoi Semyachik, Uzon caldera) Kamchatka [73,74].

Variations in cumulative proportions of the principal types of metal and mineral microinclusions in lavas from the frontal-arc Mutnovsky and rear-arc Gorely and Bakening are summarized in Figure 14. Mutnovsky lavas contain the least amount of native precious and base metals, and their alloys and gold-bearing compounds were not detected in the studied samples. Acanthite, Cu-Ag sulfides and Ag-Cl (± Cu) microinclusions dominate microinclusion assemblages in low-K tholeiitic lavas from the Mutnovsky volcano (Figure 14).

The textural appearance of several sulfides, chlorides and Cl-S-bearing compounds of chalcophile metals (Figures 8B and 9H) indicates their post-magmatic origin, which, together with the occurrence of secondary carbonates and zeolites in Mutnovsky lavas, may record post-eruptive mineral transformations caused by the intense fumarolic activity. Mutnovsky volcano hosts a large and very active fumarolic system [57] manifested at the surface with several fumarolic fields enriched in carbon dioxide, sulfur and chlorine [38]. Fumarolic sublimates at the Mutnovsky volcano contain a diverse population of Ag-Pb-Cd-Bi-bearing sulfides and chlorides, Pb-Bi-As sulfosalts, and Pb-Bi sulfohalides [39,58], along with various sulfates, such as alunite, jarosite and baryte [59]. Orthopyroxene-hosted inclusions of magmatic baryte are observed in basaltic andesites from the Mutnovsky volcano (Figure 11B,C), and both magmatic and post-magmatic baryte types are present in the Gorely and Bakening basalts, andesites and dacites (Table 2; Figure 14). Relative scarcity of native metals and alloys in the Mutnovsky lavas (Figure 14) is consistent with slightly oxidized conditions (+0.9 to +1.7 ΔQFM based on sulfur isotope measurements in melt inclusions [63]) inferred for their differentiation in shallow magmatic conduits in the arc crust beneath southern Kamchatka [56,57].

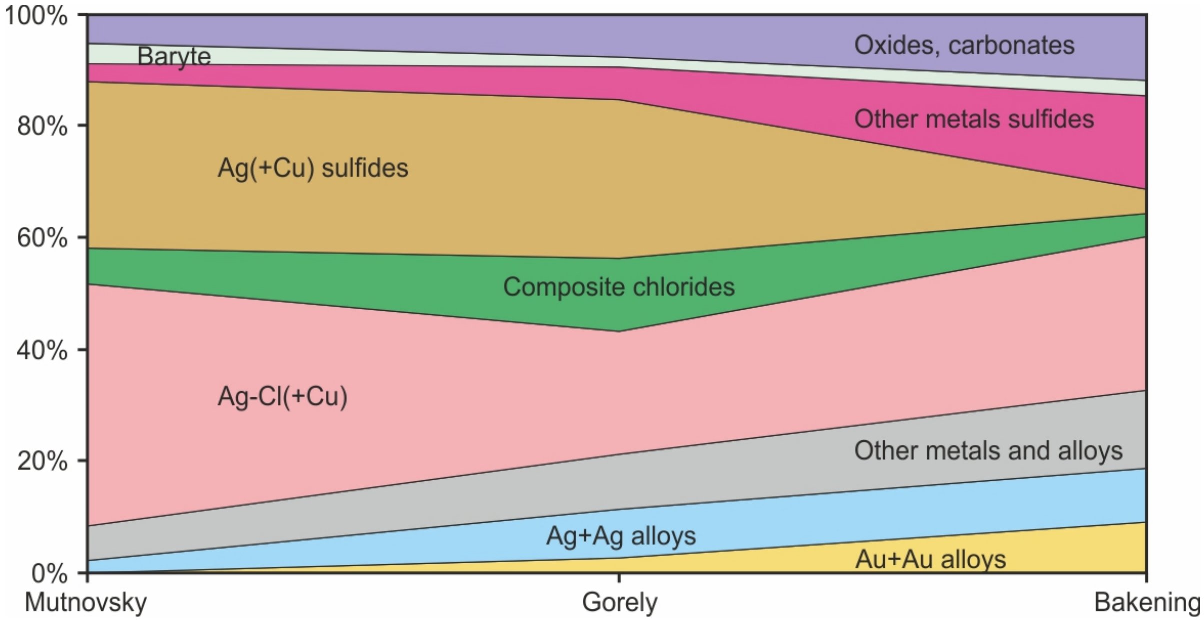

Figure 14. Cumulative proportions (%) of metal and mineral microinclusions in Quaternary lavas from the Mutnovsky, Gorely and Bakening volcanoes in Kamchatka. Data sources: Gorely [67]; Bakening [68].

5.3. Comparison with Epithermal and Porphyry Mineralization in Kamchatka

The long-lived Mutnovsky eruptive center is spatially associated with several proximal epithermal Au-Ag and porphyry-type Cu-Au ore showings [30,75]. Several types of metal and mineral microinclusions in Mutnovsky lavas are found as typomorphic ore minerals in epithermal and porphyry mineralization throughout the Kamchatka metallogenic province (Table 3). For example, cupriferous silver, acanthite, Cu-Sn (natural bronze) and Cu-Zn (natural brass) alloys; chlorargyrite, frequently in association with native silver; and composite Cu-Ag sulfides are found both in Mutnovsky samples and Kamchatka epithermal and porphyry ores (Table 3). Magnetite, titanite, apatite, baryte and zeolites are also present both as microminerals in the Mutnovsky lavas and as ore macrominerals in the epithermal and porphyry mineralization in Kamchatka (Table 3).

Table 3. Comparison of ore microminerals in Mutnovsky lavas with mineralogy of epithermal and porphyry deposits in Kamchatka.

Volcano/Deposit Type	Ore Minerals and Microminerals	Host and Associated Minerals
Mutnovsky volcano	**Cu-Ag, Cu-Sn and Cu-Zn alloys; native Ag; Cag**; Cu-Ag-Cl, Zn-Ag-Cl, Cu-Ag-Cl-S, Zn-Cu-Ag-Cl-S compounds; **Cst**	Ol; **Cpx**; Opx; **Pl**; **Ano**; **Ab**; **Qz**; **Ap**; **Ti-Mag**; **Mag**; **Ttn**; **Brt**; **Zeo**
Epithermal deposits	Py; Gn; Sp; **Aca**; **Cag**; Tnt-Ttr; native Au and Ag; Au-Ag, **Cu-Ag**, **Cu-Sn and Cu-Zn alloys**; Au, Ag and Pb tellurides, selenides, bismuthites and antimonides; Ag, Sn, Sb and As sulfosalts; Ccp; Bn; Cct; Cv; Apy; Sbn; **Cu-Ag sulfides**; Au, Ag, Pb and Bi sulfides; native Cu; **Cst**	**Qz**; **Cal**; Adl; Alu; Kln; **Ano**; Or; **Pl**; **Ab**; Ms; Chl; Ep; Act; Ser; **Ap**; **Mag**; **Brt**; Anh; Zeo
Porphyry deposits	Py; Po,; Ccp; Cct; Bn; Dg; native Au (± Cu, Pd); **Cu-Ag alloys**; Sp; **Cu-Ag sulfides**; platinum-group minerals; Gn; Mol; **Cst**; Mlc; Azu	Bt; Or; Cpx; **Pl**; Ab; Ep; Act; Rt; Hem; **Mag**; **Ap**; Chl; **Ttn**; Cal; Kln; Anh; **Brt**

Note. Similar minerals in Mutnovsky lavas and epithermal and porphyry deposits in Kamchatka are shown in bold. Data sources: Mutnovsky, this study; epithermal [5,76–79] and porphyry [30,75] deposits in Kamchatka. Mineral abbreviations: Ab—albite, Aca—acanthite, Act—actinolite, Adl—adularia, Alu—alunite, Anh—anhydrite, Ano—anorthoclase, Ap—apatite, Apy—arsenopyrite, Azu—azurite, Bn—bornite, Brt—baryte, Cag—chlorargyrite, Cal—calcite, Ccp—chalcopyrite, Cct—chalcocite, Chl—chlorite, Cpx—clinopyroxene, Cst—cassiterite, Cv—covellite, Dg—digenite, Ep—epidote, Gn—galenite, Hem—hematite, Kln—kaolinite, Mag—magnetite, Mlc—malachite, Mol—molybdenite, Ms—muscovite, Ol—olivine, Opx—orthopyroxene, Or—orthoclase, Pl—plagioclase, Py—pyrite, Qz—quartz, Sbn—stibnite, Ser—sericite, Sp—sphalerite, Ti-Mag—titanomagnetite, Ttn—titanite, Zeo—zeolites. Identical minerals are shown in bold.

Besides the obvious similarities mentioned above, there are clear differences between microinclusion assemblages in the Mutnovsky volcano lavas and the ore mineralogy of the proximal and more distant epithermal and porphyry deposits in the Kamchatka region. Native gold and gold-based alloys (with Ag, Cu and Pd) are principal mineral phases in Kamchatka Au-Ag deposits, along with pyrite, galena, sphalerite, Au-Ag-Pb tellurides, selenides, bismuthites and diverse species of sulfosalts of chalcophile metals and metalloids [5,30]. None of these phases have been detected so far among microminerals in the Mutnovsky lavas (Table 3). Porphyry systems in Kamchatka are dominated by chalcopyrite, bornite, chalcocite, pyrite and pyrrhotite along with minor galena, sphalerite, molybdenite, malachite and azurite (Table 3). Composite chlorides and sulfide–chlorides of chalcophile metals are the most common magmatic and post-magmatic microinclusions in Mutnovsky lavas; however, with the exception of minor chlorargyrite in some supergene epithermal mineralization, they are quite scarce in Au-Ag deposits and showings in Kamchatka. Acanthite, which is common among Mutnovsky microinclusions, occurs in some Ag-rich epithermal deposits, such as Rodnikovoe near the Mutnovsky volcano and Baranievskoe in Central Kamchatka [77,78], but is absent from the porphyry mineralization in this region (Table 3).

Although all these mineralogical comparisons are quite general, approximate, and perhaps even far-reaching, we hypothesize that assemblages of microinclusions in magmatic (orthopyroxene and plagioclase) and late-magmatic (amphibole and anorthoclase) minerals from Mutnovsky lavas record early (magmatic) stages of formation of related hydrothermal ore systems. These systems—provided the right set of ore-forming conditions is available—might develop potentially economic mineralization in the upper parts of the subarc crust that underlies volcanoes of South Kamchatka [73,79]. Ore microminerals in the Mutnovsky lavas, as well as in some other volcanic rocks from Kamchatka [30,40,67,68], can be interpreted as geochemical “building blocks”, which can be transported by the metal-rich fluids exsolved from arc-related tholeiitic and calc-alkaline magmas and incorporated into the developing mineralized hydrothermal cells beneath the modern and paleo-volcanic edifices throughout the Kamchatka metallogenic province.

5.4. Inferences on the Nature of the Associated Fluid

Evolution and metallogenic characteristics of volcanic arc magmas are, to a significant extent, controlled by the composition of the associated fluid phase [22,27,80]. Many primary magmatic, late-magmatic and post-magmatic microinclusions in Mutnovsky lavas contain variable amounts of sulfur and chlorine in composition, which suggests their formation from the S- and Cl-bearing fluids and melts. Occurrence of texturally primary sulfide (Figures 8A,C and 9A,C,D,F) and baryte (Figure 11B,C) microinclusions in such magmatic minerals as orthopyroxene and Ca-plagioclase indicates that sulfur could have been present in the microinclusion-forming melt or fluid as sulfide and sulfate ions, depending on the redox conditions [24,81]. The presence of cerussite microinclusions in plagioclase and groundmass volcanic glass in basaltic andesite (Figure 10D,E) possibly indicates the presence of carbon dioxide in magmatic volatiles that accompanied magmatic differentiation of the parental Mutnovsky melt. This is consistent with elevated levels of CO_2 measured in gas emissions from the active crater and fumarolic fields at the Mutnovsky volcano [39]. In general, assemblages of magmatic, late-magmatic and post-magmatic microinclusions in Mutnovsky lavas appear to reflect the composition of C-O-S-Cl-bearing volcanic gases measured instrumentally at the active vents of this long-lived eruptive center in South Kamchatka [38,39,57].

5.5. Implications for the Metallogeny of Low-K Tholeiitic Magmas in Volcanic Arcs

Metallogeny of volcanic arc magmas results from a complex interplay of many factors, including local and regional tectonics, subducted slab age and nature of associated fluid fluxes, composition and thickness of the overriding lithosphere, as well as conditions of magma generation and fractionation (recharge and storage) in crustal magmatic plumbing systems [4,7,11,13,20,25,26,82,83]. Calc-alkaline and adakitic magmas in modern and ancient active margins are typically associated with Cu-Au-Mo porphyry and Au-Ag epithermal deposits primarily due to their elevated water contents and general oxidized nature [6,14,16,19,21,27,30]. Metallogeny of low-K arc tholeiites is still not very well understood, although some tholeiitic volcanic series associated with subduction initiation in the Semail ophiolite are characterized by enrichment in selected chalcophile elements and appear to be associated with Cyprus-type volcanogenic massive sulfide (VMS) mineralization [84]. Low-K tholeiitic basalts and basaltic andesites in the ancestral Cascade arc (40–25 Ma) display elevated Cu contents and are locally associated with the small-scale, low-grade, porphyry-style copper mineralization [85].

Quaternary lavas from the Mutnovsky volcano exhibit subtle enrichment in selected chalcophile elements (Mo, Ag, Sn, Sb, Pb) with differentiation (Figure 5). In addition, concentrations of tin, antimony and silver (Table 1) in Mutnovsky samples are slightly higher than in typical calc-alkaline eruptive centers in the Eastern Volcanic Front (EVF; Figure 1) of Kamchatka [67,86]. This is consistent with the high solubility of these metals in S-Cl-bearing magmatic volatiles [12,13,62,87], which accompany the evolution of parental basaltic melts in magmatic conduits beneath southern Kamchatka [88]. Distribution of ore elements in Quaternary lavas from the Mutnovsky volcano, normalized to the bulk continental crust [89] in Figure 15, was compared with the average compositions of Kamchatka adakites [68], calc-alkaline lavas from the Kamchatkan active volcanic front [86], and arc tholeiites from the Semail ophiolite complex in Oman [84]. The majority of the Mutnovsky samples are enriched in Cu and variably depleted in Zn, As, Sn (with the exception of dacite MTN-1 with Sn = 2.65 ppm; Table 1) and Pb in reference to the bulk continental crust (Figure 15). All Mutnovsky lavas display a prominent positive silver anomaly, which is consistent with the presence of various types of Ag-bearing microinclusions (alloys, chlorides, sulfides; Figure 14) in their magmatic and post-magmatic silicate minerals. Mutnovsky samples also display extremely low Cu/Ag ratios (<350) in comparison with N-MORB (3000–4000), which suggests deep early fractionation of the sulfide phase (most likely, monosulfide solid solution, MSS; [90]) during high-pressure fractionation of the parental basaltic magma at the base of the thick (~35–38 km; [91]) subarc crust beneath the Mutnovsky volcano. The average Kamchatka adakite is characterized by the highest Ag concentrations among all Cenozoic rocks in this volcanic province (Figure 15), which is consistent with a wide range of Ag-bearing microminerals (native Ag, Ag-Au and Cu-Ag-Au alloys, cupriferous silver, acanthite, chlorargyrite, etc.) observed in Miocene–Pliocene adakites from central and northern Kamchatka [68,88]. In addition to prominent silver (and to a lesser extent, copper) enrichment in the tholeiitic series from the Mutnovsky volcano, all volcanic rocks (tholeiitic, calc-alkaline, and adakitic) from Kamchatka, along with subduction initiation-related tholeiites from the Semail ophiolite in Oman, display a positive Sb anomaly in the continental crust-normalized ore element patterns (Figure 15). Experimental data indicate that antimony will accumulate in differentiating arc-related melts within the wide range of temperatures and oxygen fugacity values and that any Sb loss through degassing during magmatic differentiation will be quite limited [92]. This is, at least to a certain extent, supported by the elevated Sb concentrations in Mutnovsky andesite and dacite (0.66 and 0.40 ppm, respectively; Table 1); the presence of the late- or post-magmatic Sb oxide in plagioclase from Mutnovsky basalt (Figure 10C); and the occurrence of Sb-bearing (±Pb, Cu, and Zn) oxychlorides and sulfides in basalt and ankaramite from the Kuril (Alaid volcano) and Kamchatka (Avachinsky volcano) volcanic arcs [88].

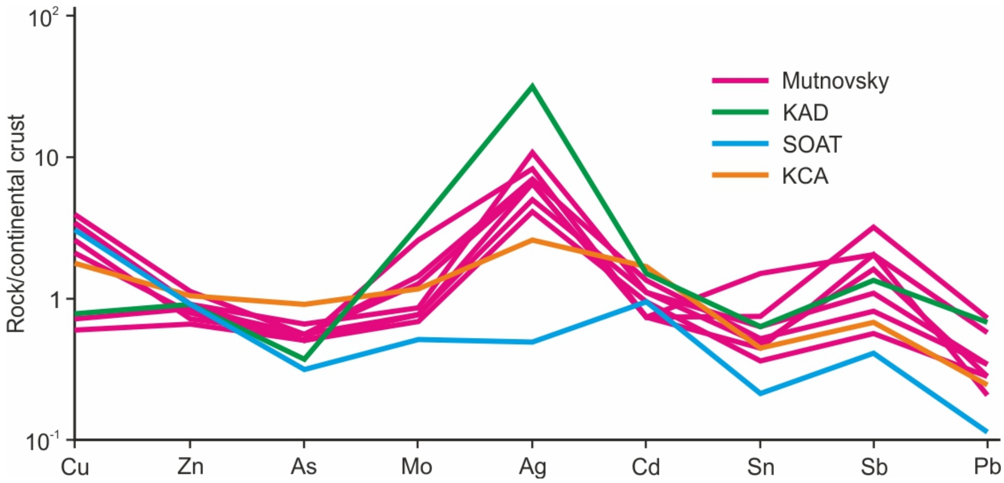

Figure 15. Distribution of ore elements in Quaternary lavas from the Mutnovsky volcano compared to the average Kamchatka adakite (KAD) [68], the Semail ophiolite arc tholeiite (SOAT) in Oman [84], and Kamchatka calc-alkaline (KCA) volcanic rocks [86]. Normalizing values for the bulk continental crust are from [89].

Mutnovsky volcano is associated with the very large and active geothermal system expressed in high-temperature (>600 °C) fumaroles in the active crater, numerous thermal water springs, mud pods and other related hydrothermal phenomena [57]. Mutnovsky volcanic gases are enriched in chlorine, sulfur and carbon dioxide [38]. Chlorine-rich (salinity up to 4465 mg/L) geothermal waters at Mutnovsky contain poorly soluble iodargyrite (AgI), naumannite (Ag_2Se) and electrum [93]. Mutnovsky thermal springs are enriched in Ag, Sb, Hg, Au, and As with respect to the El Chichon, Etna, Vulcano and Ebeko (Kuriles) hydrothermal systems [94], which is consistent with Sb and Ag enrichment in the Quaternary Mutnovsky lavas analyzed in this study (Figure 15). These data suggest high fluid exsolution efficiency of Mutnovsky and nearby Gorely magmas with respect to some chalcophile metals and gold, which is manifested by the occurrence of several high-grade epithermal Ag-Au (±Cu, Sb, and Sn) deposits and showings around these hydrothermally active volcanic centers in southern Kamchatka [67,75,78,93,95].

6. Conclusions

1. Low-K tholeiitic basalts and basaltic andesites from the Mutnovsky volcano are products of 15–26% partial melting of a depleted mantle wedge source beneath southern Kamchatka. Andesites and dacites were either formed through crystal fractionation of parental basalt or through partial melting of a garnet-free basaltic protolith in the subarc crust.
2. Basalt, basaltic andesite, andesite and dacite lavas contain microinclusions of Cu-Zn-Sn-Ag alloys, acanthite, composite Cu-Ag and Cu-Zn-Ag sulfides and chlorides,

along with Sn-Sb-Bi oxides and baryte. Proportions of Cu-Ag sulfide microminerals and bulk concentrations of Cu, Ag, Sn, Sb and Pb increase from basalt to dacite, potentially reflecting incompatible behavior of some chalcophile elements during magmatic differentiation.

3. Mutnovsky lavas are characterized by higher cumulative proportions of Cu-Ag chlorides and sulfides in comparison with calc-alkaline magma series in both frontal-arc and rear-arc volcanoes in the Kamchatka arc. The predominance of chalcophile metal chlorides and sulfides and enrichment of Mutnovsky volcanic rocks in Cu, Ag and Sb may indicate involvement of S-Cl-bearing fluids in crustal evolution of Kamchatka arc tholeiite magmas.
4. Assemblages of microminerals in Mutnovsky lavas display certain similarities with ore mineral associations of epithermal and porphyry deposits in Kamchatka, which suggests that low-K tholeiitic magmas may be potentially linked to the evolution of magmatic–hydrothermal ore-forming systems beneath active and dormant volcanoes at convergent plate margins.

Author Contributions: Conceptualization, N.P., P.K. and N.B.; methodology, N.P., P.K. and N.B.; software, N.P.; validation, N.P., P.K. and N.B.; formal analysis, N.P.; investigation, N.P., P.K. and N.B.; resources, N.P., P.K. and N.B.; data curation, P.K.; writing—original draft preparation, N.P., P.K. and N.B.; writing—review and editing, N.P., P.K. and N.B.; visualization, N.P.; supervision, P.K.; project administration, P.K. and N.B.; funding acquisition, N.B. All authors have read and agreed to the published version of the manuscript.

Funding: This research was funded by the Russian Science Foundation, project no. 25-17-68001 (continuation of project no. 22-17-00023). Basic financial support provided by the state assignment of the Institute of Tectonics and Geophysics, Far Eastern Branch, Russian Academy of Sciences (theme № 126020216322-5).

Data Availability Statement: Data are available upon request from the senior author.

Acknowledgments: We thank Ilya Tsoy for the preparation of petrographic thin sections and Ivan Astapov for assistance with XRF major element determinations at the Khabarovsk Innovation–Analytical Center (KhIAC), Institute of Tectonics and Geophysics, Far East Branch of the Russian Academy of Sciences (Khabarovsk, Russia).

Conflicts of Interest: The authors declare no conflicts of interest.

References

1. White, N.C.; Leake, M.J.; McCaughey, S.N.; Parris, B.W. Epithermal gold deposits of the southwest Pacific. *J. Geochem. Explor.* **1995**, *54*, 87–136. [CrossRef]
2. So, C.-S.; Dunchenko, V.Y.; Yun, S.-T.; Park, M.-E.; Choi, S.-G.; Shelton, K.L. Te- and Se-bearing epithermal Au-Ag mineralization, Prasolovskoye, Kunashir Island, Kuril island arc. *Econ. Geol.* **1995**, *90*, 105–117. [CrossRef]
3. KIlias, S.P.; Naden, J.; Cheliotos, I.; Shepherd, T.J.; Constandinidou, H.; Crossing, J.; Simos, I. Epithermal gold mineralization in the active Aegean Volcanic Arc: The Profitis Illias deposit, Milos, Island, Greece. *Mineral. Depos.* **2001**, *36*, 32–44. [CrossRef]
4. Kamenov, G.D.; Perfit, M.R.; Jonasson, I.R.; Mueller, P.A. High-precision Pb isotope measurements reveal magma recharge as a mechanism for ore deposit formation: Examples from Lihir Island and Conical seamount, Papua New Guinea. *Chem. Geol.* **2005**, *219*, 131–148. [CrossRef]
5. Bortnikov, N.S.; Tolstykh, N.D. Epithermal deposits of Kamchatka, Russia. *Geol. Ore Depos.* **2023**, *65*, 124–152. [CrossRef]
6. Henley, R.W.; Berger, B.R. Nature's refineries—Metals and metalloids in arc volcanoes. *Earth Sci. Rev.* **2013**, *125*, 146–170. [CrossRef]
7. Nadeau, O.; Stix, J.; Williams-Jones, A.E. Links between arc volcanoes and porphyry-epithermal ore deposits. *Geology* **2016**, *44*, 11–14. [CrossRef]
8. Heald, P.; Foley, N.K.; Hayba, D.O. Comparative anatomy of volcanic-hosted epithermal deposits: Acid-sulfate and adularia-serecite types. *Econ. Geol.* **1987**, *82*, 1–26. [CrossRef]

9. Boyce, A.J.; Fulignati, P.; Sbrana, A.; Fallick, A.E. Fluids in early stage hydrothermal alteration of high-sulfidation epithermal systems: A view from the Vulcano active hydrothermal system (Aeolian Island, Italy). *J. Volcanol. Geotherm. Res.* **2007**, *166*, 76–90. [CrossRef]
10. Williams-Jones, A.E.; Heinrich, C.A. Vapor transport of metals and the formation of magmatic-hydrothermal ore deposits. *Econ. Geol.* **2005**, *100*, 1287–1312. [CrossRef]
11. Richards, J.P. Magmatic to hydrothermal metal fluxes in convergent and collided margins. *Ore Geol. Rev.* **2011**, *40*, 1–26. [CrossRef]
12. Audétat, A. The metal content of magmatic-hydrothermal fluids and its relationship to mineralization potential. *Econ. Geol.* **2019**, *114*, 1033–1056. [CrossRef]
13. Grondahl, C.; Zajacz, Z. Sulfur and chlorine budgets control the ore fertility of arc magmas. *Nat. Commun.* **2022**, *13*, 4218. [CrossRef]
14. Mafra, C.; Loucks, R.; Fiorentini, M. Distinctive source and hydration state of gold-ore-forming arc magmas. *Geology* **2025**, *53*, 195–200. [CrossRef]
15. Tosdal, R.M.; Dilles, J.H.; Cooke, D.R. From source to sinks in auriferous magmatic-hydrothermal porphyry and epithermal deposits. *Elements* **2009**, *5*, 289–295. [CrossRef]
16. Costa, S.; Fulignati, P.; Gioncada, A.; Pistolesi, M.; Bosch, D.; Bruguier, O. Tracking metal evolution in arc magmas: Insights from the active volcano of La Fossa, Italy. *Lithos* **2021**, 380–381, 105851. [CrossRef]
17. Cooke, D.R.; Simmons, S.F. Characteristics and genesis of epithermal gold deposits. *Soc. Econ. Geol. Rev.* **2000**, *13*, 221–244.
18. Moncada, D.; Rimstidt, J.D.; Bodnar, R.J. How to form a giant epithermal precious metal deposit: Relationships between fluid flow rate, metal concentration of ore-forming fluids, duration of the ore-forming process, and ore grade and tonnage. *Ore Geol. Rev.* **2019**, *113*, 103066. [CrossRef]
19. Richards, J.P. The oxidation state, and sulfur and Cu contents of arc magmas: Implications for metallogeny. *Lithos* **2015**, *233*, 27–45. [CrossRef]
20. Park, J.-W.; Campbell, I.H.; Kim, J.; Moon, J.-W. The role of late sulfide saturation in the formation of a Cu- and Au-rich magma: Insights from the platinum group element geochemistry of Niuatahi-Motutahi lavas, Tonga rear arc. *J. Petrol.* **2015**, *56*, 59–81. [CrossRef]
21. Evans, K.-A.; Tomkins, A.-G. The relationship between subduction zone redox budget and arc magma fertility. *Earth Planet. Sci. Lett.* **2011**, *308*, 401–409. [CrossRef]
22. Rezeau, H.; Jagoutz, O. The importance of H_2O in arc magmas for the formation of porphyry Cu deposits. *Ore Geol. Rev.* **2020**, *126*, 103744. [CrossRef]
23. Blundy, J.; Cashman, K.V.; Rust, A.; Witham, F. A case for CO_2-rich arc magmas. *Earth Planet. Sci. Lett.* **2010**, *290*, 289–301. [CrossRef]
24. Farsang, S.; Zajacz, Z. Sulfur species and gold transport in arc magmatic fluids. *Nat. Geosci.* **2025**, *18*, 98–104. [CrossRef] [PubMed]
25. Large, S.J.E.; Nathwani, C.L.; Wilkinson, J.J.; Knott, T.R.; Tapster, S.R.; Buret, Y. Tectonic and crustal processes drive multi-million year arc magma evolution leading up to porphyry copper deposit formation in Central Chile. *J. Petrol.* **2024**, *65*, egae023. [CrossRef]
26. Tardani, D.; Tassara, S.; Sanchez-Alfaro, P.; Reich, M.; Pérez-Flóres, P.; Robidoux, P.; Contreras, C.; Pinti, D.L.; Cembrano, J.; Ague, J.J. The orientation of intra-arc crustal fault systems influences the copper budget of magmatic-hydrothermal fluids. *Commun. Earth Environ.* **2024**, *5*, 477. [CrossRef]
27. Leong, T.S.J.; Mavrogenes, J.A.; Arculus, R.J. Water-sulfur-rich, oxidized adakite magmas are likely porphyry copper progenitors. *Sci. Rep.* **2023**, *13*, 5078. [CrossRef]
28. Portnyagin, M.; Hoernle, K.; Plechov, P.; Mironov, N.; Khubunaya, S. Constraints on mantle melting and composition and nature of slab components in volcanic arcs from volatiles (H_2O, S, Cl, F) and trace elements in melt inclusions from the Kamchatka Arc. *Earth Planet. Sci. Lett.* **2007**, *255*, 53–69. [CrossRef]
29. Tolstykh, M.L.; Naumov, V.B.; Gavrilenko, M.G.; Ozerov, A.Y.; Kononkova, N.N. Chemical composition, volatile components, and trace elements in the melts of the Gorely volcanic center, southern Kamchatka: Evidence from inclusions in minerals. *Geochem. Int.* **2012**, *50*, 522–550. [CrossRef]
30. Kepezhinskas, P.; Berdnikov, N.V.; Kepezhinskas, N.; Konovalova, N. Adakites, high-Nb basalts and copper-gold deposits in magmatic arcs and collisional orogens: An overview. *Geosciences* **2022**, *12*, 29. [CrossRef]
31. Lander, A.V.; Shapiro, M.N. The origin of the modern Kamchatka subduction zone. In *Volcanism and Subduction: The Kamchatka Region*; Eichelberger, J., Gordeev, E., Izbekov, P., Kasahara, M., Lees, J., Eds.; Geophysical Monograph Series; American Geophysical Union: Washington, DC, USA, 2007; Volume 172, pp. 57–64.
32. Harbert, W.; Kepezhinskas, P.; Krylov, K.; Grigoriev, V.; Sokolov, S.; Aleksuitin, M.; Heiphetz, A.; Layer, P. Paleomagnetism and tectonics of the Kamchatka region, Northeastern Russia: Implications for development and evolution of the Northwest Pacific Basin. *Polarforschung* **2000**, *68*, 297–308.

33. Hochstaedter, A.G.; Kepezhinskas, P.K.; Defant, M.J.; Drummond, M.S.; Bellon, H. On the tectonic significance of arc volcanism in Northern Kamchatka. *J. Geol.* **1994**, *102*, 639–654. [CrossRef]
34. Ponomareva, V.; Melekestsev, I.; Braitseva, O.; Churikova, T.; Pevzner, M.; Sulerzhitsky, L. Late Pleistocene-Holocene volcanism on the Kamchatka Peninsula, Northwest Pacific Region. In *Volcanism and Subduction: The Kamchatka Region*; Eichelberger, J., Gordeev, E., Izbekov, P., Kasahara, M., Lees, J., Eds.; Geophysical Monograph Series; American Geophysical Union: Washington, DC, USA, 2007; Volume 172, pp. 165–198. [CrossRef]
35. Kepezhinskas, P.; McDermott, F.; Defant, M.J.; Hochstaedter, A.; Drummond, M.S.; Hawkesworth, C.J.; Koloskov, A.; Maury, R.C.; Bellon, H. Trace element and Sr-Nd-Pb isotopic constraints on a three-component model of Kamchatka Arc petrogenesis. *Geochim. Cosmochim. Acta* **1997**, *61*, 577–600. [CrossRef]
36. Simon, A.; Yogodzinski, G.M.; Robertson, K.; Smith, E.; Selyangin, O.; Kiryukhin, A.; Mulcahy, S.R.; Walker, J.D. Evolution and genesis of volcanic rocks from Mutnovsky Volcano, Kamchatka. *J. Volcanol. Geotherm. Res.* **2014**, *286*, 116–137. [CrossRef]
37. Selyangin, O.B. Mutnovsky volcano, Kamchatka: New evidence on structure, evolution, and future activity. *Volcanol. Seismol.* **1993**, *15*, 17–38.
38. Zelenski, M.; Taran, Y. Geochemistry of volcanic and hydrothermal gases of Mutnovsky volcano, Kamchatka: Evidence for mantle, slab and atmosphere contributions to fluids of a typical arc volcano. *Bull. Volcanol.* **2011**, *73*, 373–394. [CrossRef]
39. Zelenski, M.; Bortnikova, S. Sublimate speciation at Mutnovsky volcano, Kamchatka. *Eur. J. Mineral.* **2005**, *17*, 107–118. [CrossRef]
40. Krutikova, V.O.; Berdnikov, N.V.; Kepezhinskas, P.K. Metal and mineral microinclusions in rocks: Research finding interpretation and application to the study of magmatic systems of Kamchatka and Stanovoi fold belt. *Russ. J. Pac. Geol.* **2024**, *18*, 37–49. [CrossRef]
41. Krutikova, V.O.; Berdnikov, N.V.; Kepezhinskas, P.K. Microminerals as complimentary guides into metallogeny and the ore-forming potential of igneous rocks: Evidence from the Stanovoy superterrane (Russian Far East). *Minerals* **2025**, *15*, 504. [CrossRef]
42. Whitney, D.L.; Evans, B.W. Abbreviations for names of rock-forming minerals. *Amer. Mineral.* **2010**, *95*, 185–187. [CrossRef]
43. Warr, L.N. IMA-CNMNC approved mineral symbols. *Mineral. Mag.* **2021**, *85*, 291–320. [CrossRef]
44. Berdnikov, N.; Kepezhinskas, P.; Nevstruev, V.; Krutikova, V.; Konovalova, N. Explosive ultramafic volcanism in Phanerozoic accreted terranes: A case study of the Taragai peridotite complex (Russian Far East). *J. Asian Earth Sci.* **2025**, *281*, 106503. [CrossRef]
45. Le Bas, M.J.; Le Maitre, R.W.; Streckeisen, A.; Zanettin, B. A chemical classification of volcanic rocks based on the total alkalie-silica diagram. *J. Petrol.* **1986**, *27*, 745–750. [CrossRef]
46. Peccerillo, A.; Taylor, S.R. Geochemistry of Eocene calc-alkaline volcanic rocks from the Kastamonu area, Northern Turkey. *Contrib. Mineral. Petrol.* **1976**, *58*, 63–81. [CrossRef]
47. Irvine, T.N.; Baragar, W.R.A. A guide to the chemical classification of the common volcanic rocks. *Can. J. Earth Sci.* **1971**, *8*, 523–548. [CrossRef]
48. McDonough, W.F.; Sun, S.-s. The composition of the Earth. *Chem. Geol.* **1995**, *120*, 223–253. [CrossRef]
49. Perfit, M.R.; Gust, D.A.; Bence, A.E.; Arculus, R.J.; Taylor, S.R. Chemical characteristics of island-arc basalts: Implications for mantle sources. *Chem. Geol.* **1980**, *30*, 227–256. [CrossRef]
50. Hamada, M.; Okayama, Y.; Kaneko, T.; Yasuda, A.; Fujii, T. Polybaric crystallization differentiation of H_2O-saturated island arc low-K tholeiite magmas: A case study of the Izu-Oshima volcano in the Izu arc. *Earth Planet. Sp.* **2014**, *66*, 15. [CrossRef]
51. Hochstaedter, A.G.; Kepezhinskas, P.K.; Defant, M.J.; Drummond, M.S.; Koloskov, A.V. Insights into the volcanic arc mantle wedge from magnesia lavas from the Kamchatka arc. *J. Geophys. Res.* **1996**, *101*, 697–712. [CrossRef]
52. Gorbach, N.; Tobelko, D.; Ovsyannikov, G.; Rogozin, A.; Shcherbakov, V.; Plechova, A.; Portnyagin, M. Kronotsky Volcano—A low K end-member frontal volcano in Kamchatka: Geological structure and composition of rocks and minerals. *J. Volcanol. Geotherm. Res.* **2025**, *467*, 108430. [CrossRef]
53. Workman, R.K.; Hart, S.R. Major and trace element composition of the depleted MORB mantle (DMM). *Earth Planet. Sci. Lett.* **2005**, *231*, 53–72. [CrossRef]
54. Sun, S.-s.; McDonough, W.F. Chemical and isotopic systematics of oceanic basalts: Implications for mantle composition and processes. *Geol. Soc. London Spec. Publ.* **1989**, *42*, 313–345. [CrossRef]
55. Pearce, J.A.; Baker, P.E.; Harvey, P.K.; Luff, I.W. Geochemical evidence for subduction fluxes, mantle melting and fractional crystallization beneath the South Sandwich island arc. *J. Petrol.* **1995**, *36*, 1073–1109. [CrossRef]
56. Belovezhets, N.; Berezhnev, Y.; Abramenkov, S.; Abkadyrov, I.; Dergach, P.; Khmarin, E.; Chebrov, D.; Koulakov, I. Crustal sources of geothermal and magmatic activity in the area of Mutnovsky-Gorely volcanic complex (Kamchatka) inferred from ambient noise tomography. *J. Geophys. Res.* **2025**, *131*, e2025JB032025. [CrossRef]
57. Eichelberger, J.; Kiryukhin, A.; Simon, A. Magma-hydrothermal system at Mutnovsky volcano, Kamchatka Peninsula, Russia. *Sci. Drill.* **2009**, *7*, 54–59. [CrossRef]
58. Shevko, A.Y.; Gora, M.P.; Shevko, E.P.; Bortnikova, S.B. Forms of occurrence of metals and metalloids in products of the gas-hydrothermal activity of Mutnovsky volcano. *Dokl. Earth Sci.* **2025**, *515*, 541–545. [CrossRef]

59. Zhitova, E.S.; Khanin, D.A.; Nuzhdaev, A.A.; Nazarova, M.A.; Ismagilova, R.M.; Shilovskikh, V.V.; Kupchinenko, A.N.; Kuznetsov, R.A.; Zhegunov, P.S. Efflorescent sulphates with M^{+} and M^{2+} cations from fumarole and active geothermal fields of Mutnovsky volcano (Kamchatka, Russia). *Minerals* **2022**, *12*, 600. [CrossRef]
60. Webster, J.D.; De Vivo, B. Experimental and modeled solubility of chlorine in aluminosilicate melts, consequences of magma evolution, and implications for exsolution of hydrous chloride melt at Somma-Vesuvius. *Amer. Mineral.* **2002**, *87*, 1046–1061. [CrossRef]
61. Hui, K.; Rottier, B.; Qin, K.; Zajacz, Z.; Tsay, A.; Zhao, J.; Gao, S.; Shi, R. Silver behavior during magmatic and magmatic-hydrothermal evolution of a highly evolved reduced granitic system related to the giant Shuangjianzishan Ag-Pb-Zn-(Sn) epithermal deposit, Northeast China. *Econ. Geol.* **2024**, *119*, 59–83. [CrossRef]
62. Yin, Y.; Zajacz, Z. The solubility of silver in magmatic fluids: Implications for silver transfer to the magmatic-hydrothermal ore-forming environment. *Geochim. Cosmochim. Acta* **2018**, *238*, 235–251. [CrossRef]
63. Shishkina, T. Storage Conditions and Degassing Processes of Low-K and High-Al Tholeiitic Island-Arc Magmas: Experimental Constraints and Natural Observations for Mutnovsky Volcano, Kamchatka. Ph.D. Thesis, Universität Hannover, Hannover, Germany, 2012.
64. Borchardt, J.S.; Lee, C.-T.A. The chlorine evolution of arc magmas and the crustal water filter. *Earth Planet. Sci. Lett.* **2024**, *648*, 119048. [CrossRef]
65. Keppler, H. Experimental evidence for the source of excess sulfur in explosive volcanic eruptions. *Science* **1999**, *284*, 1652–1654. [CrossRef]
66. Ding, S.; Longpré, M.-A.; Economos, R.; Jackson, Y.; Vidal, C.-M.; Komorowski, J.-C.; Monteleone, B. Redox and magma recharge controls on excess sulfur build-up at Mount Samalas, 1257CE. *Nat. Commun.* **2025**, *16*, 9256. [CrossRef]
67. Kepezhinskas, P.K.; Potapova, N.V.; Berdnikov, N.V. Microminerals as evidence for metallogenic specialization and ore potential of Quaternary lavas from the Gorely volcano (Kamchatka). *J. Volcanol. Seismol.* **2025**, *5*, 72–88. [CrossRef]
68. Kepezhinskas, P.; Berdnikov, N.; Krutikova, V.; Kozhemyako, N. Iron-titanium oxide-apatite-sulfide-sulfate microinclusions in gabbro and adakite from the Russian Far East indicate possible magmatic links to iron oxide-apatite and iron oxide-copper-gold deposits. *Minerals* **2024**, *14*, 188. [CrossRef]
69. Pekov, I.V.; Zubkova, N.V.; Koshlyakova, N.N.; Belakovskiy, D.I.; Vigasina, M.F.; Agakhanov, A.A.; Britvin, S.N.; Turchkova, A.G.; Sidorov, E.G.; Zhegunov, P.S.; et al. Achyrophanite, $(K,Na)_3(Fe^{3+},Ti,Al,Mg)_5O_2(AsO_4)_5$, a new mineral with the novel structure type from fumarolic exhalations of the Tolbachik volcano, Kamchatka, Russia. *Minerals* **2025**, *15*, 706. [CrossRef]
70. Sandalov, F.D.; Pekov, I.V.; Koshlyakova, N.N.; Latyshev, A.V.; Zhegunov, P.S. Hematite from fumaroles of the Tolbachik volcano (Kamchatka, Russia): Chemistry, relationships with associated minerals, morphological and genetic features. *Geol. Ore Deposits* **2024**, *66*, 1145–1166. [CrossRef]
71. Pekov, I.V.; Britvin, S.N.; Agakhanov, A.A.; Vigasina, M.F.; Turchkova, A.G.; Zhegunov, P.S. Paramolybdomenite, $PbSeO_3$, a new mineral dimorphous with molybdomenite from the Tolbachik volcano, Kamchatka, Russia. *Mineral. Mag.* **2025**, 1–22. [CrossRef]
72. Nestola, F.; Kasatkin, A.V.; Biagioni, C.; Gurzhiy, V.V.; Skoda, R.; Santelio, L.; Agakhanov, A.A. Manuelarossiite, $CaPbAlF_7$, a new fluoride from the Vesuvius volcano, Italy. *Mineral. Mag.* **2025**, *89*, 133–140. [CrossRef]
73. Rychagov, S.N.; Sandimirova, E.I.; Chernov, M.S.; Kravchenko, O.V.; Sergeeva, A.V. Mineral formation at the East Pauzhetka thermal field (South Kamchtka) as an indication of influence of a deep-seated alkaline fluid and an epithermal ore-forming system. *Russ. Geol. Geophys.* **2023**, *64*, 210–230. [CrossRef]
74. Sergeeva, A.V.; Rychagov, S.N.; Kravchenko, O.V.; Sandimirova, E.I.; Nazarova, M.A.; Kartasheva, E.V.; Kuzmina, A.A. Mineral and geochemical features of zeolite-siliceous deposits at the Pauzhetka geothermal field, Southern Kamchatka. *J. Volcanol. Seismol.* **2024**, *18*, 32–47. [CrossRef]
75. Vladimirtseva, O.V.; Bergal-Kuvikas, O.; Subbotin, N.A.; Orlov, S.Y. New data on the copper mineralization of the Pribrezhny volcanic complex of Southern Kamchatka. *Russ. J. Pacific Geol.* **2025**, *19*, S99–S108. [CrossRef]
76. Okrugin, V.M.; Vymazalová, A.; Kozlov, V.V.; Laufek, F.; Stanley, S.J.; Shkilev, I.A. Svetlanite, SnSe, a new mineral from the Ozernovskoe deposit, Kamchatka peninsula, Russia. *Mineral. Mag.* **2022**, *86*, 234–242. [CrossRef]
77. Tolstykh, N.; Bukhanova, D.; Shapovalova, M.; Borovikov, A.; Podlipsky, M. The gold mineralization of the Baranyevskoe Au-Ag epithermal deposit in Central Kamchatka. *Minerals* **2021**, *11*, 1225. [CrossRef]
78. Tolstykh, N.; Shapovalova, M.; Shaparenko, E.; Bukhanova, D. The role of selenium and hydrocarbons in Au-Ag ore formation in the Rodnikovoe low-sulfidation (LS) epithermal deposit, Kamchatka Peninsula, Russia. *Minerals* **2022**, *12*, 1418. [CrossRef]
79. Borovikov, A.A.; Lapukhov, A.S.; Borisenko, A.S.; Seryotkin, Y.V. The Asachinskoe epithermal Au-Ag deposit in southern Kamchatka: Physicochemical conditions of formation. *Russ. Geol. Geophys.* **2009**, *50*, 693–702. [CrossRef]
80. Nathwani, C.; Blundy, J.; Large, S.J.E.; Wilkinson, J.J.; Buret, Y.; Loader, Y.; Tavazzani, L.; Chelle-Michou, C. A zircon case for super-wet arc magmas. *Nat. Commun.* **2024**, *15*, 8982. [CrossRef]
81. Colin, A.; Schmidt, C.; Pokrovski, G.S.; Wilke, M.; Borisova, A.Y.; Toplis, M.J. In situ determination of sulfur speciation and partitioning in aqueous fluid-silicate melt systems. *Geochem. Persp. Lett.* **2020**, *14*, 31–35. [CrossRef]

82. Kesler, S.E. Metallogenic evolution of convergent margins: Selected ore deposit models. *Ore Geol. Rev.* **1997**, *12*, 151–171. [CrossRef]
83. Sillitoe, R.H.; Perelló, J. Andean copper province: Tectonomagmatic settings, deposit types, metallogeny, exploration, and discovery. *Econ. Geol.* **2005**, *100*, 845–890.
84. Belgrano, T.M.; Milton, J.A.; Diamond, L.W.; Wolf, R.C.; Kusano, Y.; Teagle, D.A.H. Metallogeny of subduction initiation revealed by chalcophile element behavior in the Samail ophiolte. *Earth Planet. Sci. Lett.* **2025**, *667*, 119486. [CrossRef]
85. Du Bray, E.A.; John, D.A. Petrologic, tectonic, and metallogenic evolution of the Ancestral Cascades magmatic arc, Washington, Oregon, and northern California. *Geosphere* **2011**, *7*, 1102–1133. [CrossRef]
86. Liu, H.; Xiao, Y.; Sun, H.; Tong, F.; Heuser, A.; Churikova, T.; Wörner, G. Trace elements and Li isotope compositions across the Kamchatka arc: Constraints on slab-derived fluid sources. *J. Geophys. Res.* **2020**, *125*, e2019JB019237. [CrossRef]
87. Cox, D.; Watt, S.F.L.; Jenner, F.E.; Hastie, A.R.; Hammond, S.J. Chalcophile element processing beneath a continental arc stratovolcano. *Earth Planet. Sci. Lett.* **2019**, *522*, 1–11. [CrossRef]
88. Kepezhinskas, P.; Berdnikov, N.; Voinova, I.; Kepezhinskas, N.; Potapova, N.; Krutikova, V. Cl-bearing mineral microinclusions in arc lavas: An overview of recent findings with some metallogenic implications. *Geosciences* **2026**, *16*, 40. [CrossRef]
89. Rudnick, R.L.; Gao, S. Composition of the continental crust. In *Treatise on Geochemistry*; Elsevier: Amsterdam, The Netherlands, 2014; Volume 3, pp. 1–64.
90. Jenner, F.E. Cumulate causes for the low contents of sulfide-loving elements in the continental crust. *Nat. Geosci.* **2017**, *10*, 524–529. [CrossRef]
91. Moroz, Y.F.; Gontovaya, L.I. Deep structure of Kamchatka according to the results of MT sounding and seismic tomography. *Russ. J. Pacific Geol.* **2017**, *11*, 354–367. [CrossRef]
92. Fu, S.; Zajacz, Z.; Tsay, A.; Hu, R. Can magma degassing at depth donate the metal budget of large hydrothermal Sb deposits? *Geochim. Cosmochim. Acta* **2020**, *290*, 1–15. [CrossRef]
93. Skilskaya, E.D.; Sergeeva, A.V.; Zobenko, O.A.; Chernev, I.I. Geochemical characteristics and the ore potential of the Mutnovsky geothermal field, Southern Kamchatka. *J. Volcanol. Seismol.* **2025**, *19*, 435–450. [CrossRef]
94. Bortnikova, S.B.; Garvrilenko, G.M.; Bessonova, E.P.; Lapukhov, A.S. The hydrogeochemistry of thermal springs on Mutnovskii volcano, Southern Kamchatka. *J. Volcanol. Seismol.* **2009**, *3*, 388–404. [CrossRef]
95. Lattanzi, P.; Okrugin, V.M.; Corsini, F.; Ignatiev, A.; Okrugina, A.; Tschubarov, V.; Livi, S. Geology, mineralogy and geochemistry of base and precious metal mineralization in the Mutnovsky area, Kamchatka, Russia. *SEG Discov.* **1995**, *20*, 1–9. [CrossRef]